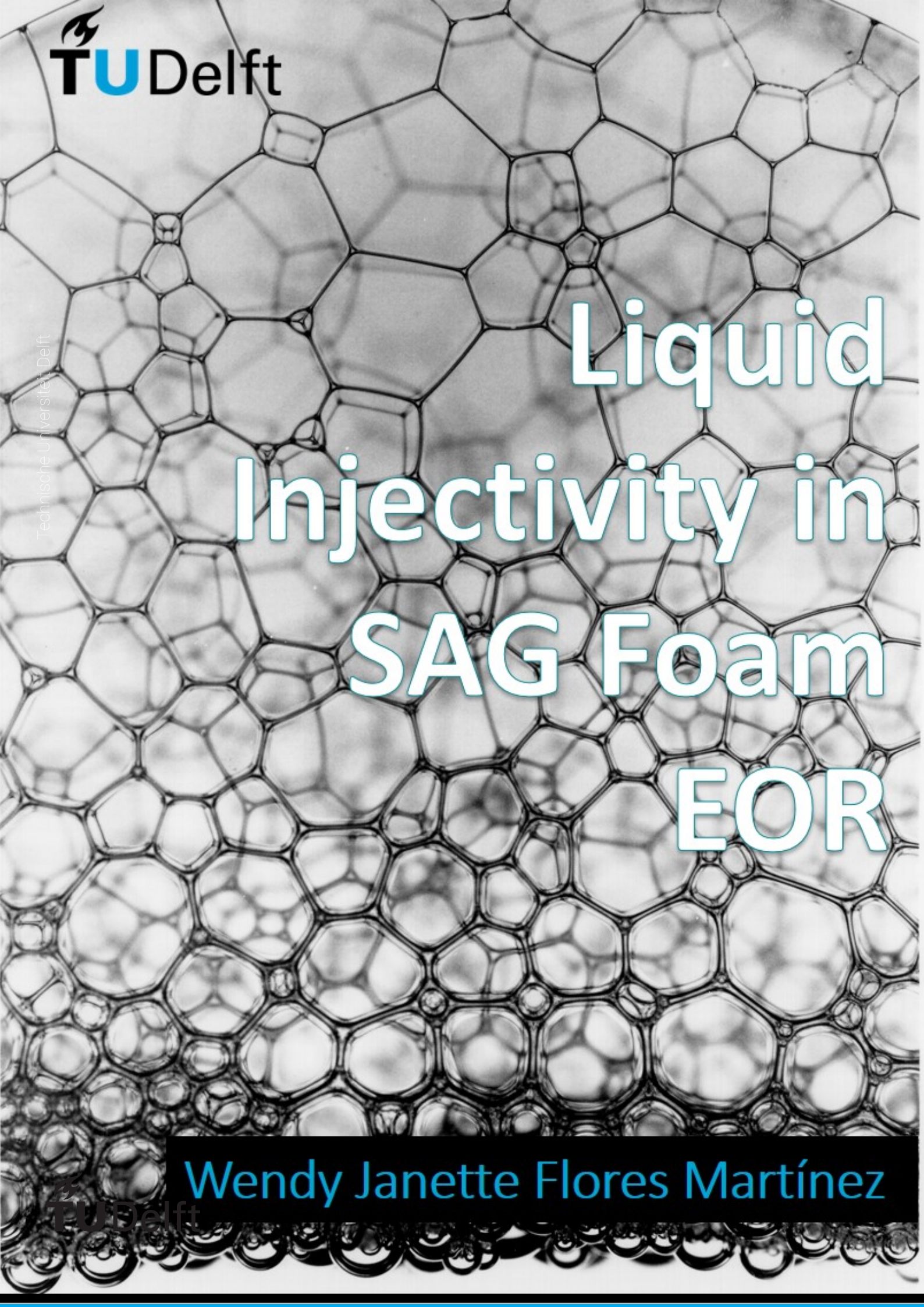
TU Delft
Technische Universiteit Delft
Liquid Injectivity in SAG Foam EOR
Wendy Janette Flores Martínez
TU Delft

Cover figure. “5% SDS in water”.
Available at: http://www.physics.upenn.edu/liugroup/jamming.html [accessed 20 August 2018]

Liquid Injectivity in SAG Foam EOR

by

Wendy Janette Flores Martínez

in partial fulfillment of the requirements of the degree of

Master of Science

in Applied Earth Sciences

at the Delft University of Technology,

to be defended publicly on Monday August 27, 2018 at 10:30 AM.

Student number:	4627520	
Supervisors:	Prof. Dr. W. R. Rossen,	TU Delft
	Dr. J. Gong,	TU Delft
	Dr. S. Vincent Bonnieu,	Shell Global Solutions B.V.
Thesis committee:	Prof. Dr. D. Voskov,	TU Delft
	Dr. K. H. A. A. Wolf,	TU Delft

TU Delft Delft University of Technology

Contents

List of Figures

List of Tables

Abstract

EOR processes employing gas injection can be very efficient in recovering oil where the gas sweeps. Unfortunately, gas injection has poor sweep efficiency because or reservoir heterogeneity, viscous instability and gravity segregation of injected gas to the top of the formation. Foam can improve the sweep efficiency in gas injection in Enhanced Oil Recovery. The best injection strategy to overcome gravity override in homogeneous reservoirs is a SAG process with a large slug of surfactant followed by a large slug of gas. An additional advantage of SAG injection is increased gas injectivity [26], water is displaced from the near-well region where foam weakens, this raises gas mobility and increases injectivity [14].However, during liquid injection, the injectivity is considered to be poor.

Liquid injectivity is not fully understood during SAG process. In this study several core-flood experiments were conducted to investigate how injectivity is affected by the injection strategy. Through these experiments, it has been found that the gas injection flow rate has no significant effect during the gas injection period, foam collapses after roughly the same number of pore volumes of gas injected regardless of the injection rate.

During the liquid injection period, liquid was injected at different flow rates following a gas injection period. The results suggested a moderately shear-thinning behaviour. Liquid injection rate was increased 10, 40 and 100 times, but the rise in pressure gradient is not proportional to the increment in injection rate.

Furthermore, the effect of the size slug injected was investigated on the subsequent liquid injection. Results show that during prolonged periods of gas injection after foam, a region near the inlet is formed in which the gas mobility is much greater and the liquid mobility is much greater than downstream during the subsequent liquid injection. The bigger the gas slug size the better the subsequent liquid injectivity in the nearest region to the inlet;

The effect of foam quality was studied; it has been found that foam quality has no big effect during the subsequent gas and liquid injections. The results of foam injection at 0.60 and 0.95 quality followed by gas injection show that foam collapsed after roughly similar number of pore volumes injected regardless of foam quality. During the liquid injection period the trends of the pressure gradient were similar at foam initial quality injection 0.60 and 0.95.

Finally, in order to verify the capability of the radial model developed by Gong et al. [7], the experimental data was fitted to the linear-flow and radial-flow models. The results suggest that the simulation based on Peaceman equation underestimated the gas and liquid injectivity in SAG process, and furthermore, the conventional simulator cannot represent the effect of gas injection on the subsequent liquid injection.

Acknowledgements

I would like to express my gratitude to my supervisor Professor Bill Rossen for the useful comments, remarks and engagement thorough the learning process of this master thesis. I would also like to give my special thanks to Dr. Jiakun Gong for his dedication, patience and understanding with my day to day work. I would like to acknowledge Dr. Sebastien Vincent-Bonnieu for sharing his knowledge and for his invaluable suggestions.

In addition, I am grateful to the members of my Msc. defence committee, Professor Karl-Heinz Wolf and Professor Denis Voskov, for reviewing this thesis and giving valuable comments. I would like to thank all the technical staff who helped me in the laboratory, especially to Michiel Slob for providing his technical expertise.

I would like to express my thankfulness to the Science and Technology Council of Mexico (Consejo Nacional de Tecnologia, CONACYT) for its financial support throughout my Master of Sciences Program.

Finally, I want to express my deepest thanks to my parents and sister, for providing me with continuous encouragement throughout my years of study.

Wendy Janette Flores Martínez

Chapter 1

Introduction

1.1 Enhanced Oil Recovery

Enhanced Oil Recovery refers to the recovery of oil due to the injection of materials that usually are not found in the reservoir but that are injected in order to alter considerably the physical-chemical behaviour of the reservoir fluids [16]. EOR implies a reduction in oil saturation below the residual oil saturation S_{or} [32].

EOR methods allow one to extract oil volumes that normally could not be obtained economically by using conventional methods and they are not restricted to a particular phase in the producing life of the reservoir [16]. These methods can be classified in two main groups: thermal (steam injection, hot water and combustion) and non-thermal (chemical injection such as surfactants, polymers and alkali and injection of immiscible gases) [32].

The target of thermal methods are heavy oils and sands, although they can be applied to light oils in special cases.These techniques supply heat to the reservoir and vaporize some of the oil. The main mechanism used by thermal methods is to reduce viscosity, other mechanisms such as rock and fluid expansion, compaction and steam distillation are also present [8].

Non-thermal methods are best suited for light oils, the two main objectives of these methods are: lowering the interfacial tension and improving the mobility ratio. Non- thermal methods can be divided in three major classes: miscible, chemical and immiscible gas injection methods [32]. EOR processes employing gas injection (miscible and immiscible solvent or steam injection) can be very efficient in recovering oil where the gas sweeps. Unfortunately, gas injection has poor sweep efficiency because or reservoir heterogeneity, viscous instability and gravity segregation of injected gas to the top of the formation [16] [31].

1.2 Foams in EOR

Foam can improve the sweep efficiency in gas injection [35][37][19]. The main reason is that foam reduces gas mobility by trapping a large fraction of the gas in place [24] [2]. Foam mobility is reduced by trapping a large fraction of gas in place, in effect reducing relative permeability of gas. [30][2][28].

Other applications of foam in porous media include:

- Acid diversion in wellbore stimulation, where foam was used to divert acid effectively from a non-damaged to a damaged zone [13].
- Low tension flood (LSF) in which foam is a substitute of polymer in Alkali Surfactant Polymer (ASP)[19].
- Recovering non-aqueous wastes from aquifers, the surfactant solution was designed to mobilize and solubilize the contaminant, which was located in the lower part of the reservoir. Then, foam was injected to produce an "in situ" foam in the zones of highest permeabilities and divert surfactant solution to the zones of lower permeability [10]
- Preventing coning of gas or water in production wells, where the objective is to eliminate or reduce the production of water during removal of working gas by blocking the flow of water into the well near the gas/water contact, this process does not require additional wells because surfactant is injected into the gas injection/production wells [36].

Foam is a dispersion of gas bubbles in a continuous liquid medium, stabilized by surfactants, where bubbles are separated by thin films called lamellae. This is thermodynamically metastable, meaning that sufficiently large external perturbation can destroy it [17].

There is a repulsion pressure called "disjoining pressure" which repels the opposite gas/liquid surfaces and depends on the surfactant formulation, temperature, pressure and other factors, these will determine the stability of the lamellae and of the foam. However, at sufficiently high capillary pressure, the films collapse in spite of the disjoining pressure [17].

1.3 SAG Foam

Foam can be placed in the reservoir by co-injection of gas and liquid at a fixed ratio of foam quality or by injection of alternating slugs of surfactant and gas (SAG). However, the best injection strategy to overcome gravity override in homogeneous reservoirs is a SAG process with a large slug of surfactant followed by a large slug of gas [33][34]. Foam is then formed when gas and surfactant come in contact in the porous medium [17] SAG injection has many advantages. It minimizes the contact between water and gas in surface facilities, this could be important if the gas forms an acid upon contact with water [27]. The injection of small volumes of gas and water can promote foam generation in the near-well region. SAG injection improves injectivity during gas injection; as water is displaced from the near-well region, water saturation declines, gas mobility increases and foam collapses, leading to an increase in injectivity [3][5]. Continuous injection should be used in order to maintain foam in the near-well region, or to ensure that gas an liquid enter to the same zone in a heterogeneous reservoir [33].

1.4 Injectivity

One of the key challenges in foam EOR process is to maintain sufficient injectivity. Injectivity controls the rate of fluid injection for a given pressure difference between the well and the reservoir; hence low injectivity decreases the injection capacity. Poor injectivity of low-mobility foam allows more time for gravity segregation of injected gas and slows the production of oil [18]. During gas injection, water is displaced from the near-well region where foam weakens, this raises gas mobility and increases injectivity [14]. Foam collapses near the injection well, giving good injectivity simultaneously with mobility control at the leading edge of the gas bank. Increased injectivity during

gas injection in a SAG process reflects high mobility near the well[17]. However during the liquid injection, injectivity can be poor in SAG which could lead to fracturing of the well [15].

Previous studies [38] [29] [23] of liquid injectivity refer a process to divert acid to desired intervals in matrix acidization treatments. In this processes the goal is to reduce the injectivity of acid into layers where less is needed and divert it into layers where is required [14]. During foam injection followed by liquid injection, pressure gradient declines in two steps. The first one occurs soon after liquid injection begins. Indirect evidence [14] [4] suggests that this decline corresponds to the displacement of mobile gas by liquid. Then, there is a second sequential decline in pressure gradient, which is attributed to dissolution of gas by unsaturated injected liquid. CT images show that during liquid injection following foam, liquid fingers through foam leaving the rest in a region [24][22]. During gas injection after foam, foam strongly weakens near the inlet of the core. In this region, the liquid saturation is low and the liquid mobility is greater during the liquid-injection period, leading to an improved swept in the core cross-section rather than a few fingers.

Liquid injectivity is poorly understood; for that reason the purpose of this thesis is to understand the injectivity during liquid injection and the effect of the injection strategy, for instance the effect of gas and liquid injection rates, gas slug size before liquid injection and the effect of permeability. Core-flood experiments were performed in order to understand liquid injectivity.

1.5 Foam Models

Design of effective foam projects requires an understanding of foam's complex behaviour. There are several methods for modelling foam in porous media. Generally these approaches are divided in two groups. Mechanistic (population balance model) foam models which represent the dynamic processes of bubble creation and destruction along with gas mobility at a given bubble size. The other group represents the effect of bubble size implicitly through a gas mobility-reduction factor that depends on water saturation, surfactant concentration and other factors. Hence there are called implicit texture (IT) models. These models assume local equilibrium between dynamic processes creating and destroying bubbles. IT models require fewer parameters and are simpler to use while population models have encountered some numerical difficulties. For purposes of this thesis, IT models are considered.

1.6 IT Models

Foam simulation parameters without oil to data for pressure gradient can be fitted as a function of gas and liquid superficial velocities [4][20]. In this method, depending on the foam quality f_g (injected gas volume fraction),high-quality and low-quality foam regimes can be identified [3][1]. In the high-quality regime, pressure gradient ∇P is nearly independent of the gas flow rate.This regime is controlled by bubble coalescence due to limiting capillary pressure $P_c{}^*$, foam rheology in this regime can be either shear-thinning or shear-thickening [4] In the low-quality regime it is shear-thinning (apparent viscosity decreases with increasing total superficial velocity). This can be explained partly by the reduction in gas trapping with increasing ∇P [3]. The transition between the regimes occurs at the foam quality $f_g{}^*$ [12]. Boeije et al [3] suggest a method for cases where data is limited: pressure gradient for one foam scan of foam quality at a fixed superficial velocity. This fitting procedure could provide an initial guess for a least-squares optimization routine.

1.7 Fitting Foam Model Parameters

STARS [9] is a widely used IT foam model. This model employs a function FM which controls the reduction in gas mobility, in Darcy's law for the gas phase.

$$u_t f_g = \frac{k k_{rg}^f}{\mu_g} \nabla p = \frac{k k_{rg} FM}{\mu_g} \nabla p$$

where:

- k_{rg} is relative permeability to gas without foam
- k_{rg}^f is relative permeability to gas with foam
- k is permeability, m^2
- ∇p is pressure gradient, Pa/m
- μ_g is gas viscosity, Pa·s
- u_t is total superficial velocity, m/s
- f_g is gas fractional flow

Function FM depends on several factors

$$FM = \frac{1}{1 + f_{mmob} * F_1 * F_2 * F_3 * F_4 * F_5 * F_6}$$

The parameter f_{mmob} is the reference gas mobility reduction factor for wet foam. Function F_1 to F_6 are restricted to values equal or less than one. F_1 models the effect of surfactant concentration, F_2 the effect of water saturation, F_3 oil saturation, F_4 gas velocity, F_5 critical capillary number and F_6 capillary number. For this study only functions F_2 and F_5 are considered.

These functions are given by

$$F_2 = 0.5 + \frac{arctan[epdry \cdot S_w - fmdry]}{\pi}$$

If $N_{ca} >$ fmcap,

$$F_5 = (\frac{fmcap}{N_{ca}})^{epcap}$$

Otherwise,

$$F_5 = 1$$

with

$$N_{ca} \equiv k \nabla p / \sigma_{wg}$$

where:

- σ_{wg} is gas/water surface tension.
- *epdry* controls the abruptness of the foam collapse.
- *epcap* captures the shear thinning behaviour of the low quality regime.
- *fmcap* is set to the smallest capillary number expected in the simulator.

- *fmdry* is equal to S_w* if the transition between the regimes is abrupt.
- S_w* is the water saturation at which foam collapses [12].

The Cheng et al method [4] requires a considerable amount of data at different gas and liquid superficial velocities to get foam-simulation parameters. Boeije et al [3], extended Cheng et al work, this method can be used when less data is available, specially a single scan of pressure as a function of foam quality at fixed total superficial velocity.

The method is as follows. Foam-free relative permeability functions $k_{rw}(S_w)$ and $k_{rg}(S_w)$ have to be known.

1. Plot the data in a ∇p versus f_g plot. Plot a straight line passing through the data at large f_g and through (1,0); for the low quality regime, plot a convex curve through the data and passing through (0,0). The intersection of the line and the curve is f_g*.
2. Fmdry can be determined from the slope of the straight line, by using Darcy's law for the aqueous phase.
3. Fmmob can be estimated from Darcy's law for gas phase by use of the value of ∇p at f_g*
4. Select a point on the curve in the low-quality regime some distance from f_g* and fit epcap to this value. Now, select fmcap and fmmob according to the range of capillary numbers expected in the simulation.
5. Select the largest value of epdry which gives acceptable simulation performance.
6. Plot the resulting fits to the low quality and high quality regime in order to verify the fit.

1.8 Effects of Gas and Liquid Velocity

Foam texture is governed by capillary pressure P_c. Liquid films or lamellae are less stable as capillary pressure increases [12], reported an abrupt transition from a strong to a weak foam at a characteristic value of capillary pressure P_c called "limiting capillary pressure". As f_g was increased, at a constant gas velocity, the capillary pressure increased [25]. At above f_g*, the foam was coarsened by increased coalescence of lamellae.

Chapter 2

Experimental description

The experimental part of this work is divided into a series of core flood experiments, which are performed in order to understand the liquid injectivity during SAG process and the influence of the injection strategy.

Below is a list of the experiments performed:

- Foam quality scan
- Effect of gas injection rate.
- Effect of liquid injection rate following gas injection.
- Effect of gas slug size on the subsequent liquid injection
- Effect of foam quality

2.1 Experimental setup and materials

Experiments were conducted in a 17-cm-long Berea sandstone core with a diameter of 3.8cm and 0.20 porosity. The permeability is 150 [mD], measured from the pressure data of brine flood through the core (see Appendix 6.1). Glue was used to encapsulate the core and avoid leaks during the experiment; the core was fitted into a PEEK core holder and placed vertically into the oven. The surfactant solution used in these experiments contained Witconate Alpha Olefine Sulfonate (AOS) surfactant, at 0.5 wt% concentration, together with synthetic seawater, which consisted of five salts:

Table 2.1: Weights of different salts used in the preparations of synthetic seawater

Salt type	Weight/Solution volume [g/l]
Calcium chloride $CaCl_2\,2\,H_2O$	2.93
Magnesium chloride $MgCl_2\,6\,H_2O$	20.30
Sodium sulphate $Na\,2\,SO_4$	7.66
Potassium chloride KCl	1.34
Sodium chloride NaCl	50.88

The experiment setup utilized to conduct the core-flood experiments consisted of a double-effect piston displacement pump (Quizix), which delivers surfactant solution at a constant flow rate, a mass flow controller (Bronkhorst), which ensures the supply of N_2 gas, also at a constant rate, a back-pressure regulator set at 40 bar to minimize the effects of the gas expansion, an oven to keep

the core at 90 °C , and a graduated cylinder to collect the effluent from the core. Pressure differences are measured along the core in five sections. Sections near the inlet and outlet are neglected during the data analysis, to avoid the capillary entry and end effects.The length of the 3 middle sections is 4.2 cm each. All the data is recorded by the MP3 software [21].

Figure 2.1 shows the setup of the experiment.

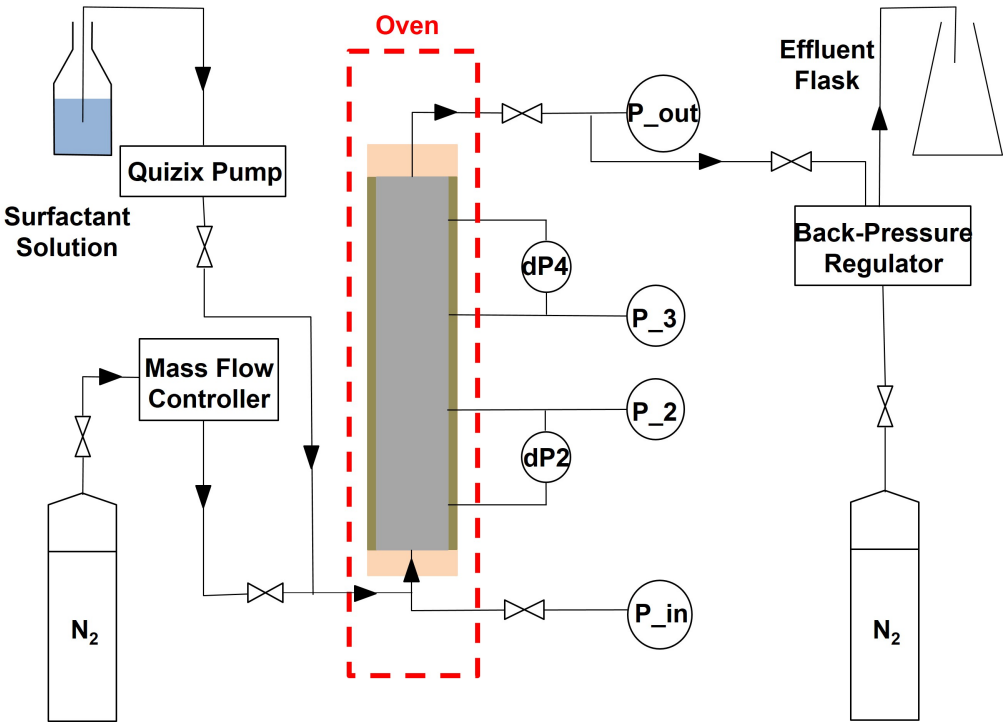

Figure 2.1: Schematic of the core flood experimental setup.

2.2 Foam quality scan

Foam quality scans are performed to identify the high-quality and low-quality regimes for the core used in the experiments. After saturating the core with surfactant solution, N_2 gas and surfactant solution were co-injected into the core at fixed flow rates. These were set to obtain a specific foam quality, f_g, such that different gas fractions are flowing through the core, while total velocity remains constant. After steady state was reached, the liquid and gas flow rates were changed to obtain a new foam quality; this represents a new point on a plot of foam quality versus apparent viscosity, similar to Figure 3.1. Steady state was considered to be reached when the recorded pressure drop remained constant over a period of time, about two hours. This process was repeated to obtain as many points as desired.

Since the Mass Flow Controller (MFC) had been calibrated at a different inlet pressure than the experimental inlet pressure the gas flow rate was corrected. For that reason the desired flow rate was multiplied by two correction factors, one for the pressure from the N_2 cylinder to the inlet of the MFC and one for the experimental pressure. A second correction with respect to gas compressibility was computed by applying the Jacobsen-Stewart equation of state; a Matlab script computed nitrogen density at standard conditions (s.c.) and at experimental conditions (e.c.); thus the real gas

superficial velocity is calculated as follows:

$$Q_{MFC} = Q_{nom} \frac{\rho_g @e.c.}{\rho_g @s.c.} CF_1 CF_2$$

where:

- Q_{MFC} is the flow rate set to the Mass Flow Controller
- $Q_{nominal}$ is the nominal flow rate
- ρ_g @e.c is the density of nitrogen at experimental conditions
- ρ @s.c. is the density of nitrogen at standard conditions
- CF_1 is the conversion factor for the MFC from 150 bar to 100 bar (0.963)
- CF_2 is the conversion factor for the MFC from 100 bar to 41 bar (0.947)

An average pressure drop measurement along each section allowed the calculation of the apparent viscosity for each section:

$$\mu_{app} = \frac{k\Delta PA}{QL}$$

where:

- μ_{app} is apparent viscosity, Pa·s
- k is permeability, m^2
- ΔP is pressure drop across core cross-sectional, Pa
- A is area, m^2
- Q is flow rate, m^3/s
- L is length of the core, m

For the Berea core, foam quality scans were conducted at 2 ft/day and 4 ft/day superficial velocities. At each total flow rate, foam qualities ranging from 0.1 to 0.99 were generated.

By applying the method of Boeije and Rossen [3] for fitting foam parameters, initial parameters were obtained. Then these values were refined by the use of the least-squares optimization Matlab routine of Farajzadeh et al.[6].

2.3 Experimental procedure for injectivity experiments

Injectivity experiments began with the core saturated with surfactant solution. Next, surfactant solution and N_2 gas were co-injected from the bottom of the core at fixed flow rates to generate 0.95-quality foam. For all the experiments the same initial foam quality was used. Once foam has reached steady state, liquid injection ceased and only N_2 gas injection continued. The aim of this first set of experiments is to study the effect of gas injection rate during the period of gas injection.

The following table shows the gas flow rates and superficial velocities used in these experiments.

Table 2.2: Gas flow rate and superficial velocity

Gas flow rate [ml/min]	Gas superficial velocity [m/s]
1	1.34e-5
2	2.68e-5
3	4.02e-5

The second set of experiments were conducted in order to test the effect of liquid injection rate following gas injection. As in the previous experiments, 0.95-quality foam was generated by co-injecting N_2 gas and surfactant solution. Once foam reached steady state, 150 pore volumes of gas were injected into the core at 2 ml/min; this weakened the foam part-way into section 2. Finally, surfactant solution was injected at different rates. This procedure was repeated at every flow rate. The table below shows the liquid flow rates and superficial velocities utilized during the experiments:

Table 2.3: Liquid flow rate and superficial velocity

Liquid flow rate [ml/min]	Liquid superficial velocity [m/s]
0.5	6.70e-6
5	6.70e-5
20	2.68e-4
50	6.70e-4

In order to test the effect of the gas slug size on the subsequent liquid injection, foam with a 0.95 gas fraction was generated. Once it reached steady state, different gas volumes were injected at 2 ml/min. After gas injection finished, surfactant solution was injected at 0.5 ml/min.

Below the gas slug sizes for this experiment are listed:

Table 2.4: Gas slug size

Gas slug size
200 PV gas injection
150 PV gas injection
50 PV gas injection
10 PV gas injection

Finally, experiments were conducted to investigate the effect of foam quality. Foam was injected at 0.60 initial quality. Similar to the previous experiments, after foam reached steady state, gas was injected at 1, 2 and 3 ml/min.

The effect of foam quality was also studied during the liquid injection period. After foam reached steady state, 150 PV of gas were injected and then liquid was injected at 0.5 ml/min and 50 ml/min.

Chapter 3

Results and discussion

3.1 Foam-quality scan

Foam scan was conducted in order to identify the low-quality regime and high-quality regimes for the core used in the experiments. Plots of gas fraction versus apparent viscosity are presented for section 4 of the core. The method of Boeije et al [3] was used to obtain a first estimate of the foam parameters by fitting the foam quality-scan at 2 ft/day and 4 ft/day, then the least-squares optimization routine of Farajzadeh et al [6] was used to refined the fit.

Figure 3.1 represents the apparent viscosity transition at 2 ft/day. As can be observed, as the gas fraction increases towards the gas critical fraction, f_g* foam apparent viscosity increases. The gas critical fraction f_g*, which corresponds to the limiting capillary pressure, establishes the transition from the low-quality regime to the high-quality regime [12]. Beyond f_g*,in the high-quality regime, the foam apparent viscosity decreases. As shown in this figure, the transition between regimes is observed at about f_g*=0.80. For our surfactant formulation, core and experimental conditions, the convex trend for $f_g < f_g$* suggests that foam behaviour is shear thinning in the low quality regime.

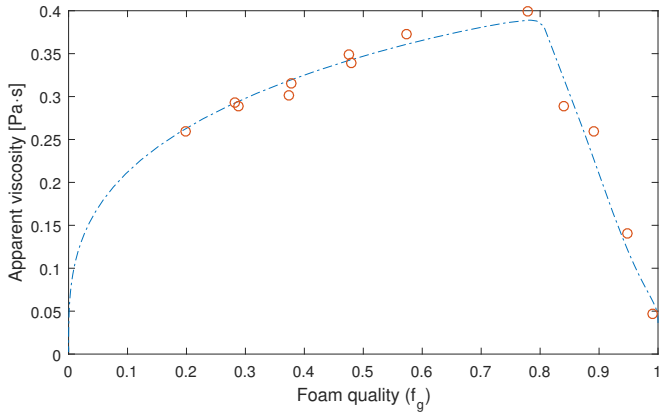

Figure 3.1: Foam fitting parameters at 2 ft/day superficial velocity

The following table provides the parameters obtained with these methods.

Table 3.1: Foam model-parameters obtained by fitting the least-square fitting approach of Farajzadeh et al. to the foam scan at 2 ft/day

Parameter	Units	Value
fmdry	-	0.342
epdry	-	963.863
fmmob	-	3.686e4
epcap	-	1.00
fmcap	-	6.1726e-6

Figure 3.2 represents the apparent viscosity as a function of foam quality at a superficial velocity 4 ft/day. The transition foam quality in this experimental data is around f_g*=0.88. The convex shape of the trend of apparent viscosity in the low-quality regime suggests that foam behaviour is near to Newtonian, but less than the data at 2 ft/day. Foam behaviour in the high-quality regime appears to be Newtonian.

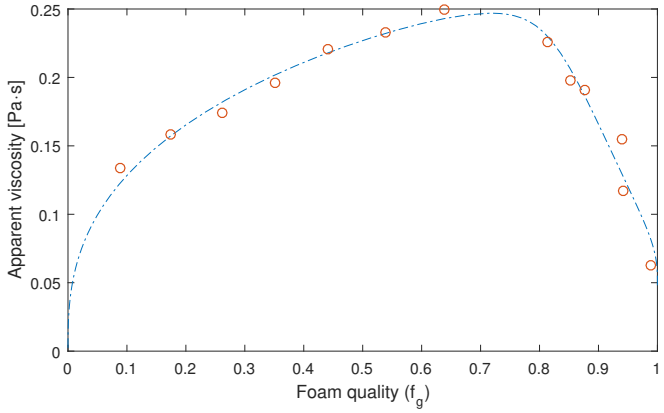

Figure 3.2: Foam fitting parameters at 4 ft/day superficial velocity

The same procedure was followed as in the previous plot in order to compute the foam parameters. Results of 4 ft/day superficial velocity are summarized in the following table:

Table 3.2: Foam model-parameters obtained by fitting the least-square fitting approach of Farajzadeh et al. to the foam scan at 4 ft/day

Parameter	Units	Value
fmdry	-	0.357
epdry	-	220.195
fmmob	-	7.877e4
epcap	-	1.360
fmcap	-	7.355e-6

The intention of these experiments is to compare the foam-scans at different superficial velocities. The transition behaviour is less sharp at 2 ft/day superficial velocity compared to 4 ft/day. The transition point f_g* appears to shift to slightly higher values at higher superficial velocities. In addition, as total superficial velocity increases, there is a reduction in apparent viscosity.

3.2 Effect of gas velocity

In order to study the effect of gas injection velocity, experiments were performed varied the gas injection velocity following foam injection. The experimental results for gas injection at different superficial velocities are presented in this section. The "local pore volume" (LPV) is defined as the

volume injected divided by the cumulative pore volume from a given position to the inlet. The "total pore volume" (TPV) refers to the total pore volume injected.

Figures 3.3, 3.4 and 3.5 show the evolution of pressure gradient during the experiments along sections 2, 3 and 4, respectively, as a function of total pore volume (TPV) injected. There is at first almost a linear decline in pressure gradient to a plateau, which is followed by a second pressure-gradient drop. When gas is injected after foam, gas mobility rises, and then holds constant, the second abrupt rise in gas mobility corresponds to a decline in water saturation, leading to a collapse of foam. The decline in water saturation is driven by the combined effects of liquid evaporation, pressure gradient and capillary effects.

Higher gas injection rates increase pressure gradient, but the increment in ∇P is not proportional to the injection rate. As can be seen in section 2 (Figure 3.3), at 1 ml/min injection rate (superficial velocity 1.676e-8 $[m^3/min]$), it takes about 190 TPV (500 LPV) of gas injection to dry-out the foam. When the injection rate is doubled, the number of TPV required to weaken the foam is around 140 TPV (360 LPV), and when the injection rate is tripled, foam collapses after 130 TPV (340 LPV). There is a moderate difference with respect to the number of pore volumes required to collapse foam at different injection rates.

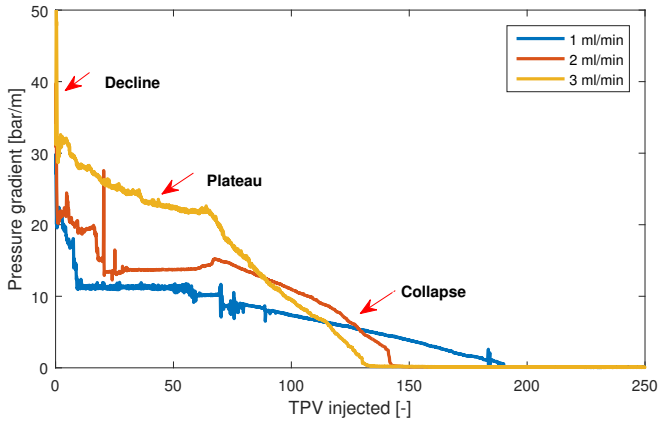

Figure 3.3: Pressure gradient profile along section 2 during gas injection following foam. Gas injection at 1, 2 and 3 ml/min

A similar trend is observed in section 3. The lowest injection rate, 1 ml/min, seems to take more pore volumes to collapse foam, followed by 2 ml/min (superficial velocity 3.353e-8 $[m^3/min]$) and 3 ml/min (superficial velocity 5.029e-8 $[m^3/min]$).

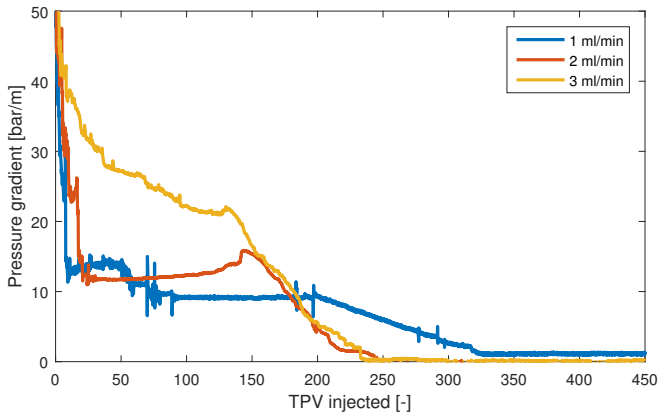

Figure 3.4: Pressure gradient profile along section 3 during gas injection following foam. Gas injection at 1, 2 and 3 ml/min

Figure 3.5 represents pressure evolution in section 4. The difference in the number of pore volumes injected at the point of foam collapse is again moderate. Some spikes can be observed, especially in pressure gradient at 2 ml/min and 1 ml/min. These were caused by fluctuations in the back-pressure regulator. The trends in these figure are similar to each other except that the injection rate is twofold and threefold higher; however, foam does not collapse two or three times faster. Evaporation has an important effect in the foam collapse during long periods of gas injection. As more gas is injected, liquid evaporates, first weakening foam and then causing the collapse of the foam.

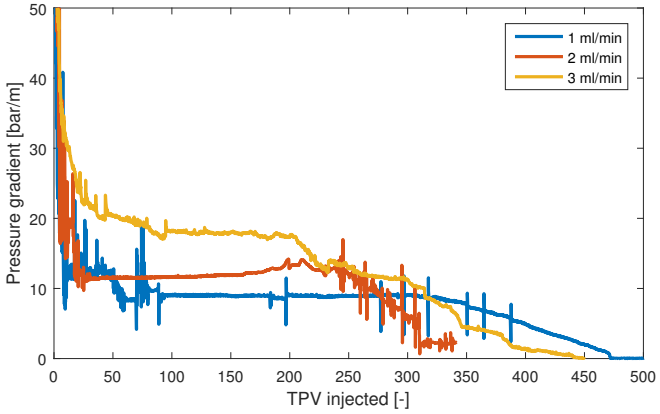

Figure 3.5: Pressure gradient profile along section 4 during gas injection following foam. Gas injection at 1, 2 and 3 ml/min.

Figures 3.6, 3.7 and 3.8 show the pressure profile in terms of local pore volumes (LPV) for all three sections in each experiment. During gas injection at 1 ml/min, Fig. 3.6, section 2 seems to dry-out faster than sections 3 and 4, after about 500 LPV. The foam-collapse bank propagates with a similar velocity in each section.

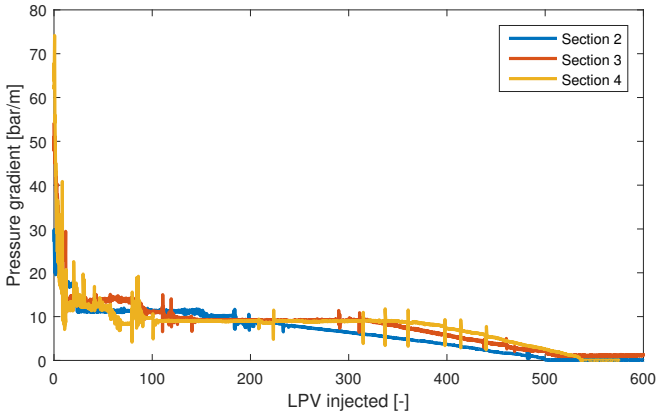

Figure 3.6: Gas injection at 1 ml/min flow rate in terms of local pore volumes

For 2 ml/min superficial velocity, Fig. 3.7, the foam-collapse region reaches the end of each section after about 380 LPV gas injection. All sections have a similar propagation velocity.

Fig. 3.8 represents pressure transition along the core at 3 ml/min injection rate. Foam did not collapse after the same number of LPV; the region of collapsed foam propagates faster in section 2. The main reason is that the core is not completely homogeneous, there is s small difference in the measured permeability in each section: 161 mD for section 2, 157 mD for section 3 and 140 mD for section 4. That could lead to slightly different propagation velocities at each section.

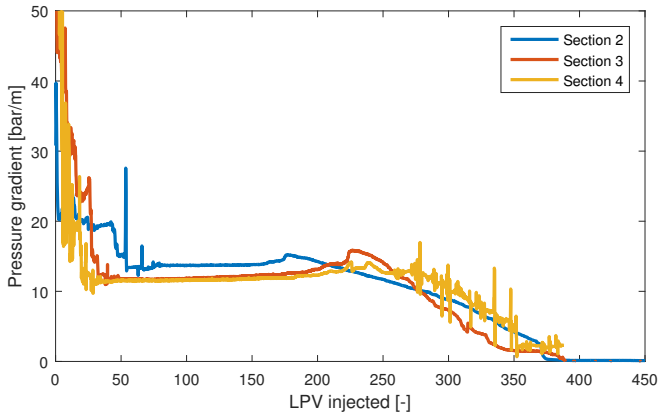

Figure 3.7: Gas injection at 2 ml/min flow rate in terms of local pore volumes

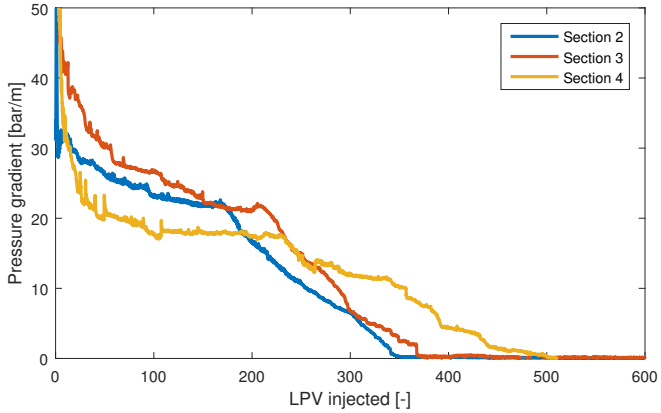

Figure 3.8: Gas injection at 3 ml/min flow rate in terms of local pore volumes

As discussed, gas velocity has no strong impact on foam collapse. During gas injection, foam at first does not collapse; the plateau in pressure gradient corresponds to the foam weakening, the second decline represents foam collapse or greatly weakening. The trend suggests somewhat a shear-thinning behaviour. Higher injection velocities increase pressure gradient but the increment is not proportional to the increment in superficial velocity. For instance, the injection velocity was doubled and tripled but the increase in the plateau value of pressure gradient was not two or three times higher. The second pressure-gradient decline started roughly after the same number of pore volumes gas injected. Then foam completely collapsed after 550 pore volumes at the lowest superficial velocity while at the highest superficial velocity foam collapsed after approximately 445 pore volumes gas injection. These values do not reflect the increase in superficial velocity. Results show that the foam-collapse region propagates faster in some sections of the core. The reason could be that there is a small difference in the measured permeability in each section which lead to slightly different propagation velocities at each section.

If water was displaced only by the the effect of pressure gradient then the increment in injection velocity would lead to a proportional increment in pressure gradient. If water was displaced only by evaporation then pressure gradient would be independent of the increment in injection velocity. Results show he foam collapse reflects the effect of pressure driven flow, capillary effect and an important effect of liquid evaporation. As more gas is injected, liquid evaporates, first weakening foam and then causing the collapse of the foam.

3.3 Effect of liquid velocity

The objective of these experiments is to investigate the effect of liquid superficial velocity during liquid injection. After foam was generated, 150 TPV of gas were injected. During gas injection, as shown in Fig. 3.9, foam collapsed or greatly weakened in section 2; this corresponds to the end of the second decline in pressure gradient after 150 TPV. The foam-collapse region is part-way through sections 3 and 4.

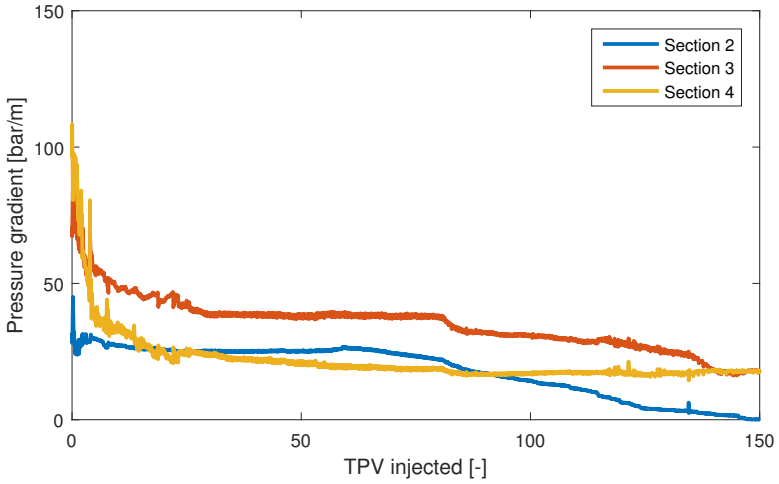

Figure 3.9: Pressure gradient profile during 150 TPV gas injection at 2 ml/min

After gas injection finished, surfactant solution was injected in to the core at different flow rates. Figure 3.10 shows pressure gradient in section 2. This is the region nearest to the inlet; during liquid injection there is a quick rise in pressure gradient, followed by a plateau, at 0.5 ml/min the plateau is wider but as injection rate increases the plateau becomes shorter. Lastly, after the plateau there is a gradual decline in pressure gradient. The trend suggests a moderately shear-thinning behaviour. Liquid injection rate was increased 10, 40 and 100 times, but the rise in pressure gradient during the plateau is not proportional to the increment in injection rate. For instance, the peaks of pressure gradient at 50 ml/min and 0.5 ml/min are at 120 bar/m and 10 bar/m, respectively.

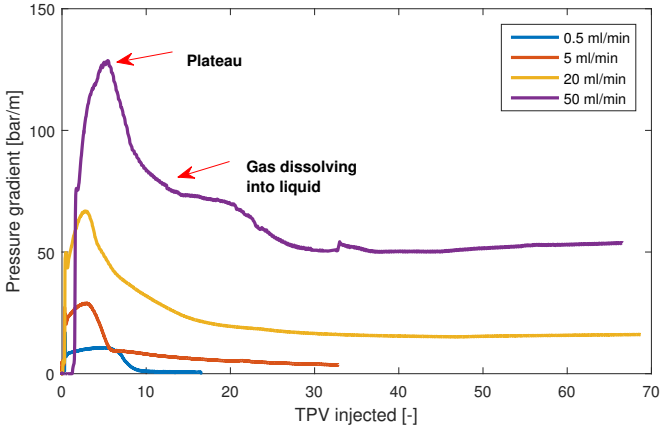

Figure 3.10: Pressure gradient along section 2 as a function of TPV injected during liquid injection at different injection rates

Similar results are seen in section 3 (Figure 3.11) and 4 (Figure 3.12). Pressure gradient rises to a plateau followed by a drop. Comparing the three sections, the peaks of pressure gradients are considerably smaller in section 2 than in the other two sections. As shown in Figure 3.9, after 150PV of

gas injected, foam collapsed in section 2. This has an effect on the subsequent liquid injection in section 2, it reduced considerably pressure gradient in this region.

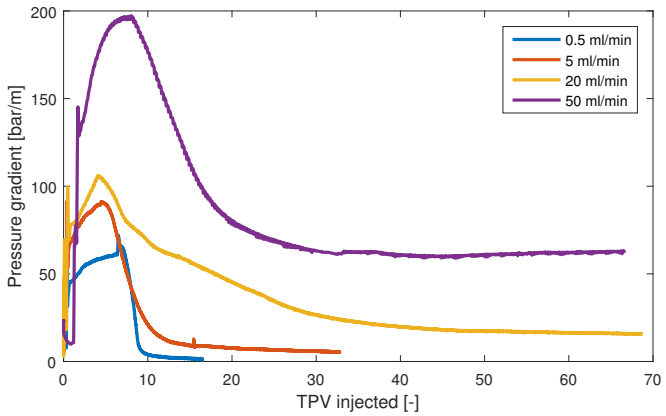

Figure 3.11: Pressure gradient along section 3 as a function of TPV injected during liquid injection at different injection rates

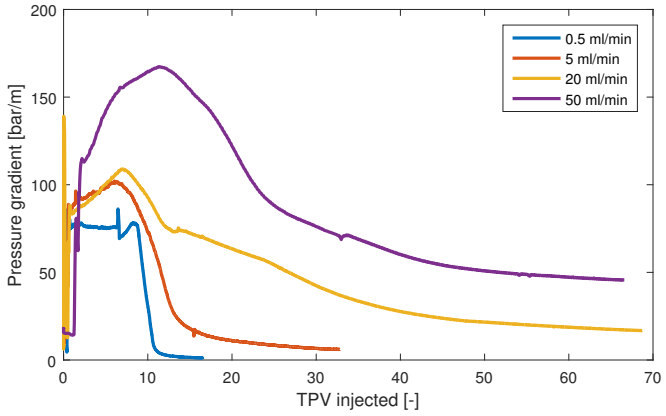

Figure 3.12: Pressure gradient along section 4 as a function of TPV injected during liquid injection at different injection rates.

Gas injection affects the subsequent liquid injection especially in the region near the inlet (section 2). In the weakened-foam region (sections 3 and 4) pressure gradient is not significantly affected by the amount of gas previously injected. Soon after the liquid injection begins, pressure gradient increases to a plateau, this occurs in the foam-collapsed region. Then there is a second decline attributed to dissolution of gas by liquid [14][27], followed by a much lower steady pressure gradient value corresponding to the liquid fingering through the foam. As liquid injection rate increases, more gas could be dissolved in liquid and then it is expected that liquid fingers through the foam in a wider area.

The experimental results for the gas injection period show the effect of increasing injection velocity. The trend suggests a shear-thinning behaviour. The liquid injection velocity increased 10, 40 and 100 times but the increment in pressure gradient was only 3, 7 and 13 times, respectively. Soon after liquid injection begins, there is a quick rise in pressure gradient, followed by a plateau where liquid mobility holds constant. As the liquid injection rate increases, the plateau becomes shorter in terms of liquid pore volumes. The plateau corresponds to the liquid saturating the foam-collapsed region. Then there is decline in pressure corresponding to the dissolution of gas in liquid fingers followed by a lower pressure value representing the liquid fingering region. The mobility in the plateau is roughly similar to the area of the finger times the relative permeability to water in the finger, which

is approximately ten times greater at the highest pressure gradient. Relative permeability to water in finger is inversely related to gas saturation in finger. The region nearest to the inlet is quite sensitive to the gas slug previously injected, pressure gradients are much lower in this section than in the furthest region. Regardless of the velocity, the dissolution of gas in liquid starts roughly after the same number of pore volumes liquid injected.

3.4 Effect of gas slug size on subsequent liquid injection

Previous studies suggest that during long periods of gas injection after foam, a region near the inlet is formed in which the gas mobility is greater. The abrupt rise in gas mobility appears to reflect the decline of water saturation below about 0.20 [7]. In this region, foam is completely collapsed or strongly weakened; then during the subsequent liquid injection, the liquid mobility is much greater and liquid sweeps the entire cross-section rather than one or few fingers [7]. During the liquid-injection period, the pressure gradient is strongly affected by the size of the slug previously injected. Figure 3.13 shows the pressure gradient during liquid injection following gas injection in section 2, which is the nearest section to the inlet. After 150 PV of gas injected, foam is completely collapsed or strongly weakened in section 2. A small volume of gas, 10PV gas injection, does not improve the subsequent liquid injectivity much. It weakens foam only in a small region in the section. As the gas slug size increases from 10 PV to 200 PV, the pressure gradient during subsequent liquid injection decreases from approximately 70 [bar/m] to 5 [bar/m].

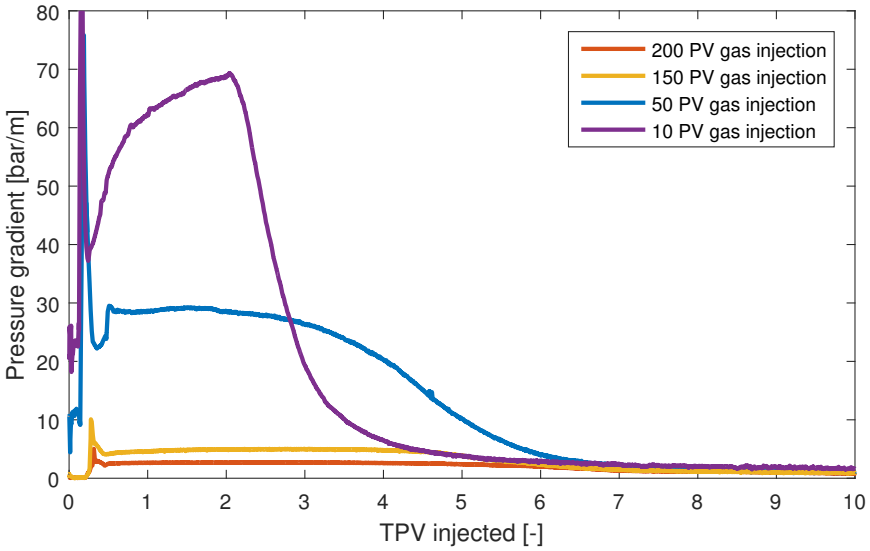

Figure 3.13: Pressure gradient profile along section 2 during liquid injection following gas injection.

Figure 3.14 illustrates the pressure-gradient profile along section 3. The collapsed foam has not penetrate this section totally even after 200 PV gas injection. During liquid injection, after 10 PV gas injection, the pressure gradient is approximately 80 [bar/m] while it is about 50 [bar/m] after 200 PV gas injection. Pressure gradient in section 3 is higher than in section 2 where injectivity is greatly affected by the size of the gas slug previously injected. This seems to indicate that gas slug has a moderate effect on this section 3. The plateau lasts longer as more gas was injected.

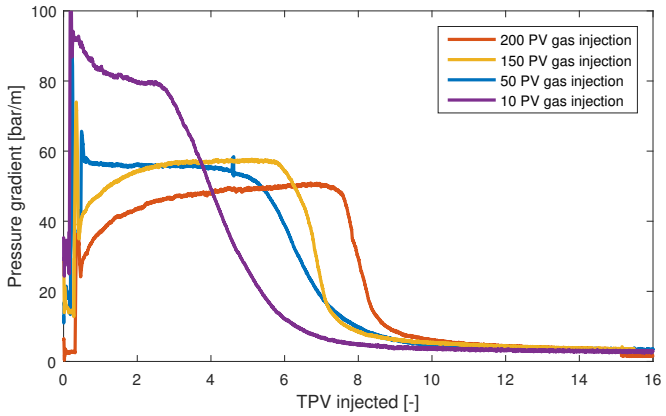

Figure 3.14: Pressure gradient profile along section 3 during liquid injection following gas injection.

Figure 3.15 shows the pressure gradient in section 4 during liquid injection. The pressure gradient is roughly the same regardless of period of gas injection, around 80 [bar/m]. However, the plateau becomes longer as more gas is injected; the longest plateau is observed after 200 PV gas injection, while the shortest is after 10 PV gas injection.

Apparently liquid injectivity is not improved in this section; the pressure gradient is relatively insensitive to the gas-slug size previously injected.

As gas is injected in the core, foam collapses in the nearest region to the inlet. The size of this region depends on the gas-slug size injected. Beyond the collapsed-foam region, foam is partially weakened. There, during liquid injection, gas is dissolved in liquid, this corresponds to the decline in pressure gradient. Finally the the lowest steady value of pressure gradient correspond to the liquid fingering through the foam. In the region where foam is not collapsed, the plateau value of pressure gradient tends to last longer for larger gas slugs.

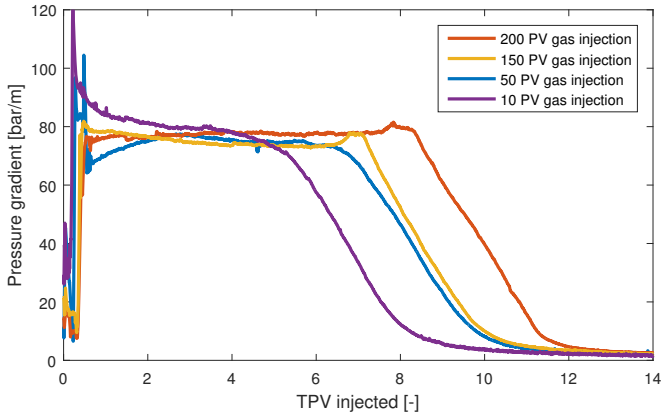

Figure 3.15: Pressure gradient profile along section 4 during liquid injection following gas injection.

Pressure gradient during liquid injection is strongly affected by the size of the gas slug previously injected in the nearest region to the inlet. The bigger the gas slug size, the better the subsequent liquid injectivity. Beyond the foam-collapsed region, the effect of the gas slug size is not visible, liquid holds constant until gas within the fingers dissolves into liquid. Th plateau value of pressure gradient is similar for different gas slug sizes but it tends to last longer for larger gas slugs. This suggests that it takes longer for liquid to dissolve the gas within the fingers if more gas was injected previously. Is is expected that liquid fingers are wider if liquid is injected at a higher velocity. As shown, the larger the gas slug size previously injected, the smaller the pressure gradient in the following

liquid injection, which corresponds to an increase in liquid injectivity.

3.5 Effect of foam quality

Experiments were conducted to investigate the effect of foam quality on the subsequent liquid and gas injections. Fig.3.16 and 3.17 compare the pressure gradient in section 2 during gas injection at different velocities following 0.60 and 0.95 quality foam, respectively .The first quality is in the low-quality regime and the second in the high-quality regime. Data is available only for section 2 because the trend suggested that there was no significant difference between both qualities and continuing the experiments would have required a lot of time. In general, higher pressure gradients are observed during gas injection following 0.60-quality foam.

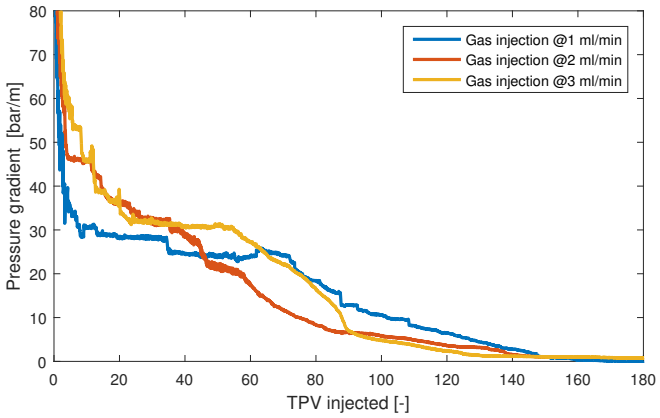

Figure 3.16: Pressure gradient in section 2 during gas injection at different superficial velocities following foam injection at 0.60 quality

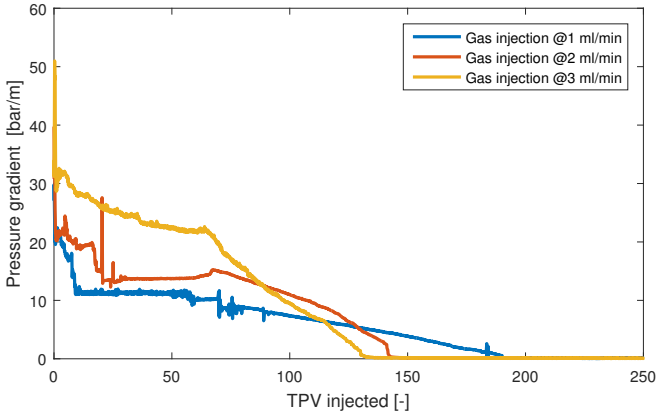

Figure 3.17: Pressure gradient in section 2 during gas injection at different superficial velocities following foam injection at 0.95 quality

Figures 3.18, 3.19 and 3.20 show the same data but now comparing both qualities during each gas injection rate. During gas injection at 1 ml/min, foam collapsed after around 170 PV following 0.60-quality foam while 0.95-foam quality collapsed after 190 PV. The trends are similar for 2 ml/min and 3 ml/min injection rates. Following the plateau, there is a gradual pressure gradient drop when foam has finally collapsed. There is not a considerable difference with respect to the number of pore volumes required to collapse foam with both foam qualities, foam collapse seems to be insensitive to the initial foam quality previously injected.

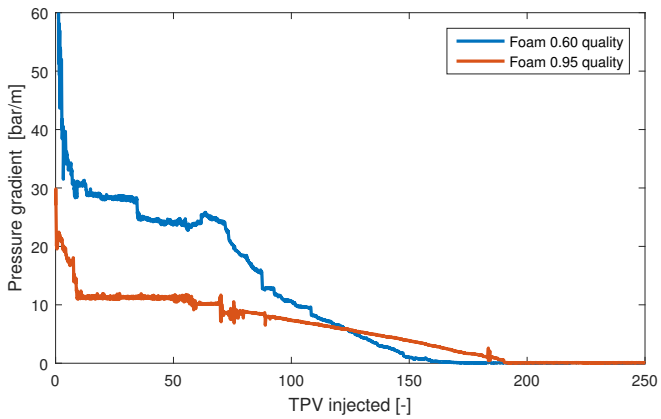

Figure 3.18: Pressure gradient as a function of TPV injected during gas injection at 1 ml/min.

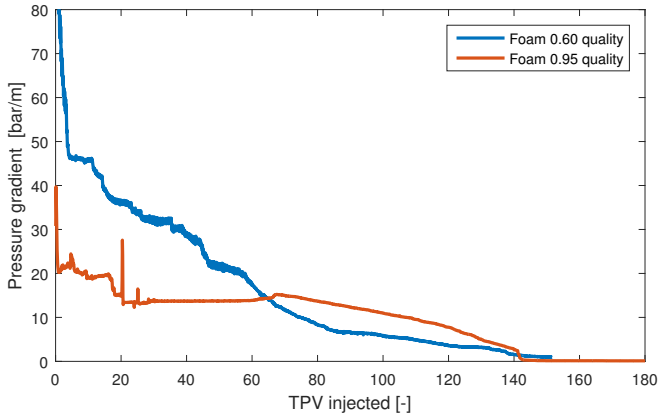

Figure 3.19: Pressure gradient as a function of TPV injected during gas injection at 2 ml/min.

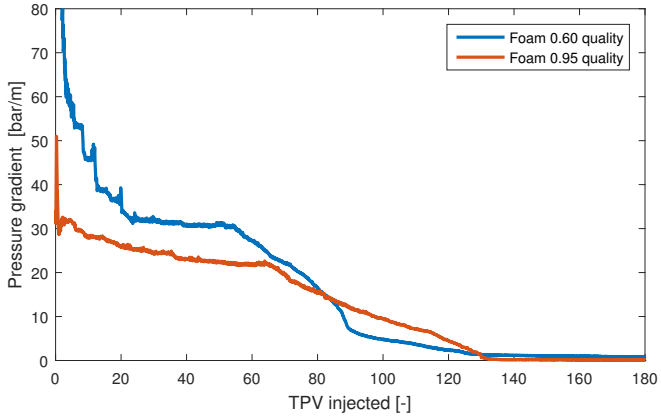

Figure 3.20: Pressure gradient as a function of TPV injected during gas injection at 3 ml/min.

Figure 3.21(a) shows the pressure gradient transition during liquid injection at 0.5 ml/min injection rate following 150 PV gas injection after 0.60 and 0.95 foam qualities in section 2. Pressure gradient seems to be similar with both initial qualities. There is sudden increase in pressure gradient to a plateau followed by a sharp pressure gradient decline. Similar behaviour is observed during liquid injection at 50 ml/min. (3.21(b)). Liquid injection appears to be insensitive to the foam quality previously injected; the difference between pressure gradient with 0.95 and 0.60 foam quality is small. The plateau becomes shorter as the liquid injection rate increases for both qualities.

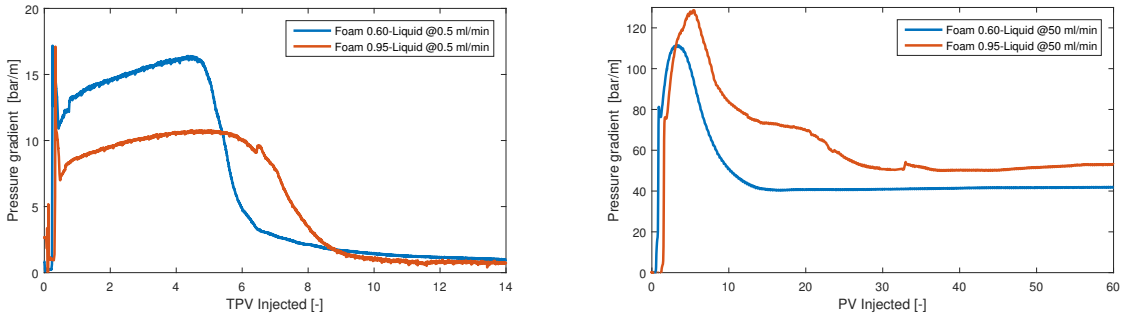

(a) Liquid injection at 0.5 ml/min superficial velocity

(b) Liquid injection at 50 ml/min superficial velocity

Figure 3.21: Pressure gradient in section 2 during liquid injection at 0.5 ml/min (3.21(a)) and at 50 ml/min (3.21(b)) following 150 PV gas injection, following injection of foam 0.60 and 0.95 quality.

Figure 3.22 compares the pressure gradients in section 3 during liquid injection after 150 PV gas injection following injection of foam 0.95 and 0.60 quality. As shown in figure 3.22(a) liquid injection is not affected by the initial foam quality; the difference in pressure gradient is moderate. This trend is visible also with a higher injection rate.

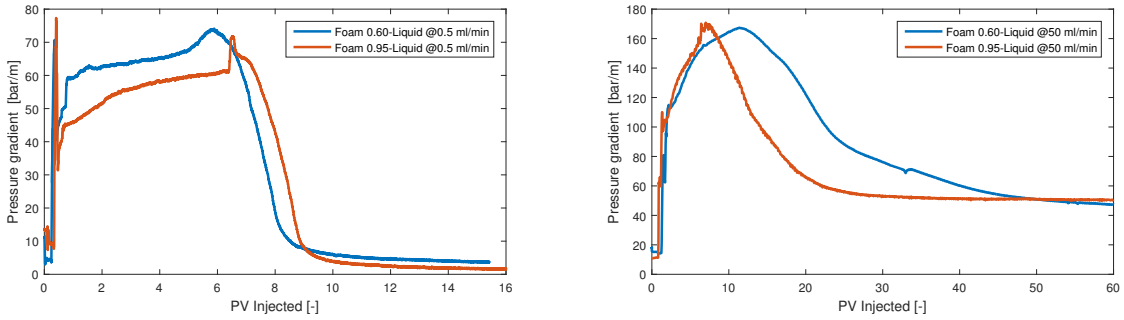

(a)

(b)

Figure 3.22: Pressure gradient in section 3 during liquid injection at 0.5 ml/min (3.22(a)) and at 50 ml/min (3.22(b)) following 150 PV gas injection, following injection of foam 0.60 and 0.95 quality.

Figure 3.23 shows the initial foam quality does not affect significantly the subsequent liquid injection. Pressure gradient is moderate for this section as well. The plateau values are similar for both qualities at 0.5 ml/min, around 80 bar/m. During liquid injection at both flow rates, there is no considerably difference in the pore volumes liquid injected to dissolve gas in section 4.

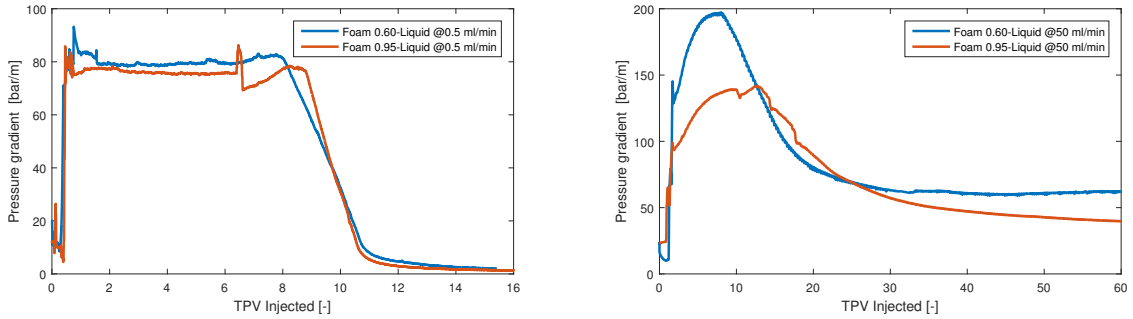

(a) Liquid injection at 0.5 ml/min superficial velocity

(b) Liquid injection at 50 ml /min superficial velocity

Figure 3.23: Pressure gradient in section 4 during liquid injection at 0.5 ml/min (3.23(a)) and at 50 ml/min (3.23(b)) following 150 PV gas injection, following injection of 0.60 and 0.95 quality.

Experiments conducted at different initial foam quality reflect that liquid and gas injection periods are insensitive to the foam quality previously injected. Foam 0.60 and 0.95 quality represent the low-quality regime and the high-quality regime, respectively. In the beginning, the maximum pressure gradient during gas injection following 0.60 foam quality are higher than that foam 0.95-quality foam. Thereafter, foam collapses after similar number of pore volumes gas injected. During liquid injection following 150 PV gas injection following foam 0.60 and 0.90 quality, the values in pressure gradient are higher with 0.60 foam-quality. After approximately the same number of pore volumes liquid injected, gas starts to dissolve in liquid, this corresponds to the decline in pressure gradient at the end of the plateau. The liquid injection and gas injection periods are insensitive to the foam quality previously injected.

Chapter 4

Modelling of Liquid Injectivity

Based on core-flood experiments, Gong et al [7] developed a model to describe liquid and gas injectivity. The model describes the propagation of various banks during liquid and gas injection. First a linear model was developed for the gas injection and the subsequent liquid injection in a SAG process. The dimensionless propagation velocities and mobilities of the various banks are calculated from the experimental data; these are inputs of the linear-flow model and the radial-flow model. The position of the fronts are calculated in terms of local pore volumes (LPV) and the total mobilities of the banks are assumed to be uniform in each bank. The "local pore volume" (LPV) is defined as the volume injected divided by the cumulative pore volume from a given position to the inlet. For instance, during gas injection at 1 ml/min, the foam-collapse region reaches the end of the section after approximately 550 LPV. Therefore the foam-collapse bank propagates with a dimensionless velocity: V=1/550.

4.1 Linear Flow Model

The experimental results during the gas-injection period suggest that the injectivity in a SAG process is driven by two banks, as illustrated in Figure 4.1.

Figure 4.1: Banks during gas injection period in a SAG process. The foam bank is initially in place and then the foam-collapse bank advances forward.

During the liquid-injection period, injectivity is described by the propagation of the following banks:

Figure 4.2: Banks during liquid injection period in a SAG process. The foam bank and the foam-collapse bank are initially present. The liquid-fingering and the gas-dissolving banks advance into the foam bank.

For the gas-injection period in a SAG process, the total pressure difference is the sum of the pressure differences of the foam bank in the foam-collapse bank (as long as each bank is represented in the section of the core of interest.[7]:

$$\Delta P_t = \Delta P_F + \Delta P_{FCG}$$

For the liquid injection period, the total pressure difference is the sum of the pressure differences of the foam-collapse bank, the gas dissolving bank, the liquid-fingering bank and the foam bank (as long as each bank is represented in the section of the core of interest):

$$\Delta P_t = \Delta P_{FCL} + \Delta P_{GD} + \Delta P_{LF} + \Delta P_F$$

Pressure gradient, reported below, is pressure difference across a given section, divided by the length of the section of the core. Darcy's law for linear multi-phase flow is used to calculate the pressure difference for each bank:

$$\Delta P_b = \int_{l_1}^{l_2} \frac{Q_t}{A\lambda_t(b)} dl = \frac{Q_t(l_2 - l_1)}{A\lambda_t(b)}$$

where

- Q_t is the flow rate
- l is the length of the section

It is assumed that the total mobility $\lambda_t(b)$ is constant in the given bank.

4.2 Results of Linear Flow Model

4.2.1 Effect of Gas velocity

Figure 4.3 shows the comparison of the results of the linear-flow model and the experimental data from gas-injection at 1 ml/min (superficial velocity 1.676e-8 $[m^3/min]$) . After about 550 LPV of gas injection, the gas mobility changes drastically, corresponding to the collapse of foam, which is reflected in a decrease in pressure gradient. The front of the foam-collapse bank advances with a dimensionless velocity 1/550. As can be observed, the model fits the experimental data well at this velocity.

Table 4.1: Propagation velocities and mobilities of the various bank estimated from lab data for gas injection at 1 ml/min.

Parameter	Value
Total mobility of foam-collapse bank [m^2/Pa·s]	3.54e-9
Total mobility of foam bank [m^2/Pa·s]	1.47e-11
Dimensionless velocity of foam-collapse bank [-]	1.82e-3

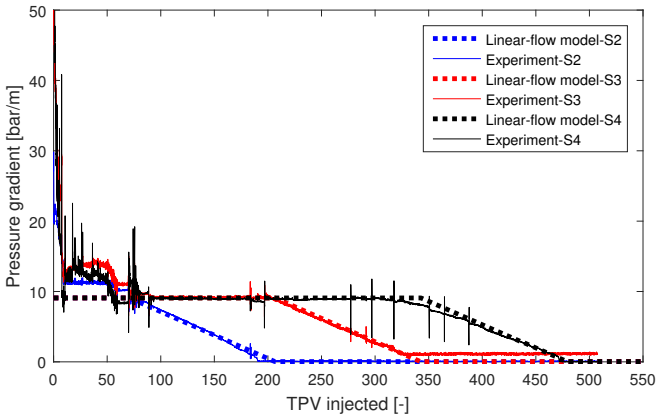

Figure 4.3: Comparison of the pressure gradient in the three sections (S2, S3, S4) of the core in the core-flood experiments and fit with the linear-flow model during gas-injection at 1 ml/min.

Figure 4.4 compares the pressure gradient in the core-flood experiments and the linear-flow model during gas injection at 2 ml/min (superficial velocity 3.357e-8 $[m^3/min]$) The front of the foam-collapse bank advances with a dimensionless velocity 1/385, which is slightly higher than the dimensionless velocity at 1 ml/min.

The linear-flow model gives a reasonable fit especially for Section 4. In sections 2 and 3 the pressure gradient starts to decline a bit later than in the model fit. The reason could be that he model assumes the same propagation velocity of the collapsed-foam bank for all three sections. In reality, foam collapse reflects the interplay of pressure gradient, capillary effects and evaporation, leading to different dimensionless velocities along the core. The injection rate was doubled but the plateau values is not twice the value plateau value of the fit at 1 ml/min. The trend suggests a bit shear-thinning behaviour.

Table 4.2: Propagation velocities and mobilities of the various bank estimated from lab data for gas injection at 2 ml/min.

Parameter	Value
Total mobility of foam-collapse bank [m^2/Pa·s]	2.77e-9
Total mobility of foam bank [m^2/Pa·s]	2.08e-11
Dimensionless velocity of foam-collapse bank [-]	2.60e-3

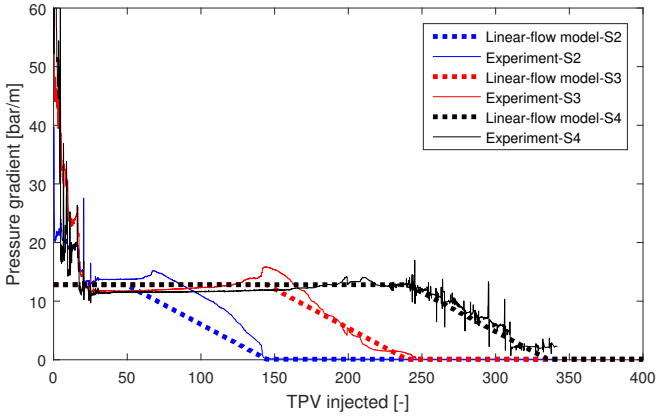

Figure 4.4: Comparison of the pressure gradient in the three sections (S2, S3, S4) of the core in the core-flood experiments and fit with the linear-flow model during gas-injection at 2 ml/min.

As can be observed in Figure 4.5, the linear-flow model provides a good fit to the data lab for gas injection at 3 ml/min (superficial velocity 5.029e-8 $[m^3/min]$). The foam-collapsed bank propagates

with a dimensionless velocity of 1/445. However, foam collapse takes shorter time in section 2 and 3. It is intended to fit the model as well as possible for section 4. Since this is the furthest region from the inlet and it is expected to be least distorted by entrance effects and other lab artifacts.

Table 4.3: Propagation velocities and mobilities of the various bank estimated from lab data for gas injection at 3 ml/min

Parameter	Value]
Total mobility of foam-collapse bank [m^2/Pa·s]	3.74e-9
Total mobility of foam bank [m^2/Pa·s]	2.16e-11
Dimensionless velocity of foam-collapse bank [-]	2.25e-3

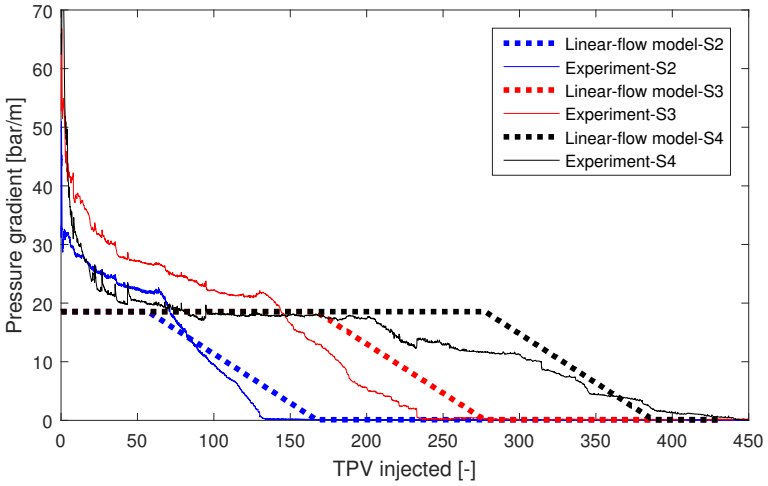

Figure 4.5: Comparison of the pressure gradient in the three sections (S2, S3, S4) of the core in the core-flood experiments and fit with the linear-flow model during gas-injection at 1 ml/min.

During gas injection, foam at first does not collapse; the plateau in pressure gradient corresponds to the foam weakening, the second decline represents foam collapse or greatly weakening. Pressure gradient declines as foam weakens in the core. However, increasing injection rate does not dry foam faster. If injection rate is twofold and threefold higher, foam does not collapse two or three times faster.

Evaporation would be expected to have an important effect in the foam collapse during long periods of gas injection. As more gas is injected, liquid evaporates, first weakening foam and then causing the collapse of the foam.

4.2.2 Effect of liquid velocity

Figure 4.6 compares the results of the linear-flow model and the experimental data during the liquid injection period at 0.5 ml/min (superficial velocity 8.333e-9 [m^3/min]) following 150 PV gas injected. The plateau values in the model are the same for Sections 3 and 4, this is because the model considers the same permeability and total mobility for all three sections, but in reality there are small differences of permeability among the sections.

Table 4.4: propagation velocities and mobilities of the various bank estimated from lab data for liquid injection at 0.5 ml/min.

Parameter	Value
Total mobility of liquid slug in collapsed-foam region [m^2/Pa·s]	4.41e-11
Dimensionless velocity of liquid slug in collapsed-foam region [-]	0.11
Total mobility of liquid fingering bank [m^2/Pa·s]	8.7e-13
Dimensionless velocity of liquid fingering bank [-]	1.47
Total mobility of gas dissolving bank [m^2/Pa·s]	2.49e-11
Dimensionless velocity of gas dissolving bank [-]	0.74

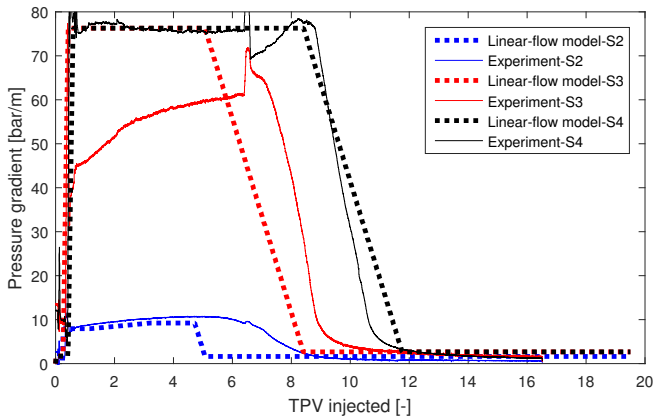

Figure 4.6: Comparison of the pressure gradient in the core-flood experiments and the linear-flow model during liquid-injection at 0.5 ml/min

Figure 4.7 shows the linear-flow model fitting to the core-flood experiment during liquid injection at 5 ml/min (superficial velocity 8.333e-8 [m^3/min]). Similar to the previous liquid flow rate, in the model the pressure-gradient plateaus are the same for sections 2 and 3 for the linear model. The model considers the ratio of the foam-collapse region with respect to the total length. The foam-collapse bank has partially penetrated section 2, where the pressure gradient is considerably lower than the other two sections. In general the model gives a reasonable fit to the lab data.

Table 4.5: Propagation velocities and mobilities of the various bank estimated from lab data for liquid injection at 5 ml/min.

Parameter	Value
Total mobility of liquid slug in collapsed-foam region [m^2/Pa·s]	8.97e-11
Dimensionless velocity of liquid slug in collapsed-foam region [-]	0.50.18
Total mobility of gas dissolving bank [m^2/Pa·s]	6,75e-12
Dimensionless velocity of gas dissolving bank [-]	1.17
Total mobility of liquid fingering bank [m^2/Pa·s]	7.62e-11
Dimensionless velocity of liquid fingering bank [-]	0.066

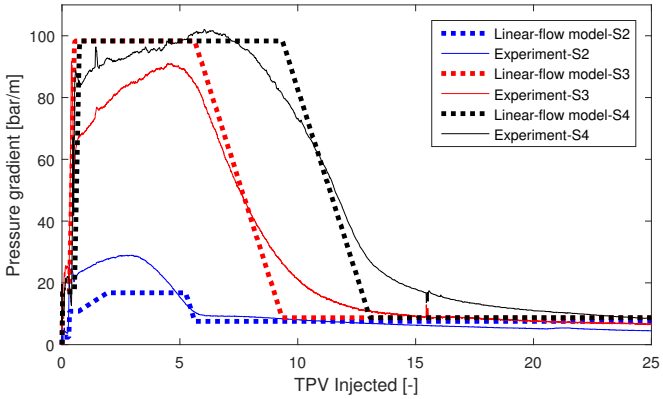

Figure 4.7: Comparison of the pressure gradient in the core-flood experiments and the linear-flow model during liquid-injection at 50 ml/min

Figure 4.8 compares the experimental data and the result of the linear-flow model at 50 ml/min liquid (superficial velocity 8.333e-7 $[m^3/min]$. As shown, the fit is not as good as for the previous flow rates. The pressure gradient in section 3 is higher than in the other two sections, and is not completely described by the model. This could be also due to a difference in permeability. The calculated mobility in the plateau at 0.5 ml/min is 4.41e-11 while at 50 ml/min is 2.31e-10, this means that mobility is approximately 5 times higher at 50 ml/min. Since the Matlab routine considers only one mobility value for the corresponding banks, mobilities and velocities are calculated as average values in each section at the corresponding flow rate. For instance, the plateau values in sections 2, 3 and 4 during liquid injection at 0.5 ml/min are 10, 55 and 75 bar/min, respectively. While during liquid injection at 50 ml/min these values are 120, 180 and 150 bar/min. This means that viscosity is only 12, 3.2 and 1.8 times lower at 50 ml/min, and average of 5 times higher mobility.

Table 4.6: Propagation velocities and mobilities of the various bank estimated from lab data for liquid injection at 50 ml/min.

Parameter	Value
Total mobility of liquid slug in collapsed-foam region $[m^2$/Pa·s]	2.31e-10
Dimensionless velocity of liquid slug in collapsed-foam region [-]	0.093
Total mobility of gas dissolving bank $[m^2$/Pa·s]	6.48e-11
Dimensionless velocity of gas dissolving bank [-]	0.037
Total mobility of liquid fingering bank $[m^2$/Pa·s]	1.05e-10
Dimensionless velocity of liquid fingering bank [-]	0.028

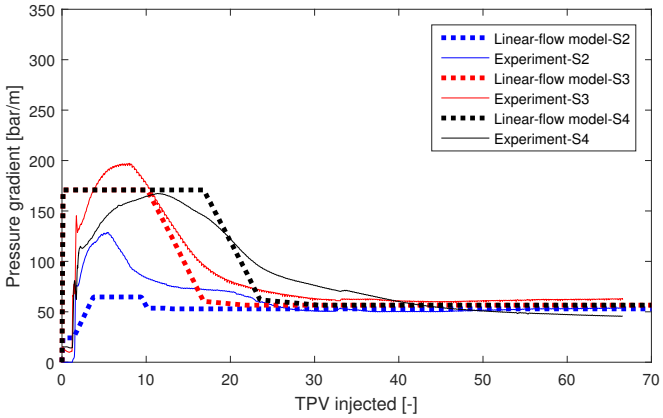

Figure 4.8: Comparison of the pressure gradient in the core-flood experiments and the linear-flow model during liquid-injection at 50 ml/min

During liquid injection following gas injection, there is a quick rise in pressure gradient, followed by a plateau and a gradual decline. The trend suggests a shear-thinning behaviour. The trend suggests a moderately shear-thinning behaviour. Liquid injection rate was increased 10, 40 and 100 times, but the rise in pressure gradient during the plateau is not proportional to the increment in injection rate.

4.2.3 Effect of size of gas slug on subsequent liquid injection

Figure 4.9 shows the comparison of the pressure gradient in the core-flood experiments and the linear-flow model during liquid injection after 200 PV of gas injection. The model gives a good fit, especially in section 4; the bank of liquid saturating the collapse-foam region seems to be larger in section 2 than the calculated by the linear model, which gives a larger plateau value of pressure gradient. The comparison to liquid injection after 150 PV of gas injection can be seen in Figure 4.10, where the fit is reasonably good. These two last experiments try to reflect the effect of the gas volume injected before the liquid injection. This is reflected in section 2, where plateau value of pressure gradient during liquid injection decreases as the volumes of gas injected increases. After 200 PV gas injected, the plateau of pressure gradient is around 4 [bar/m] while after 150 PV is approximately 10 [bar/], these two values are considerably smaller than the plateau values in section 4, where pressure gradient rises to 75 [bar/m]

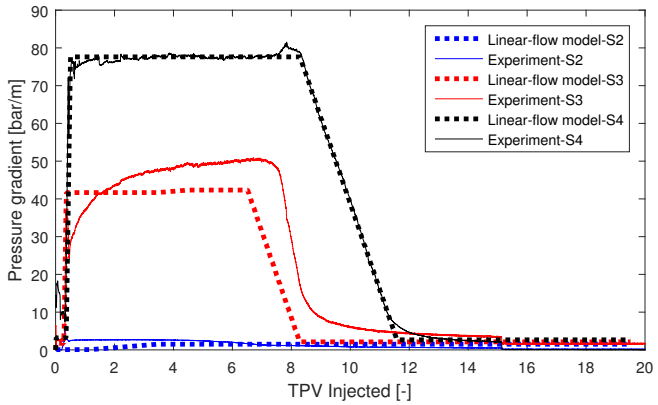

Figure 4.9: Comparison of the pressure gradient in the core-flood experiments and the linear-flow model during liquid injection after 200 PV gas injection

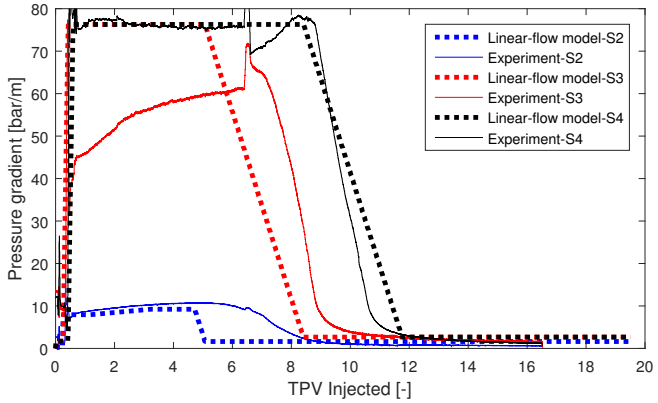

Figure 4.10: Comparison of the pressure gradient in the core-flood experiments and the linear-flow model during liquid injection after 150 PV gas injection

As gas is injected in the core, foam collapses in the nearest region to the inlet. The size of this region depends on the gas-slug size injected. The larger the gas slug size previously injected, the smaller the pressure gradient in the following liquid injection, which corresponds to an increase in liquid injectivity. Beyond the collapsed-foam region, foam is partially weakened. There, during liquid injection, gas is dissolved in liquid, this corresponds to the decline in pressure gradient. Finally the lowest steady value of pressure gradient correspond to the liquid fingering through the foam. In the region where foam is not collapsed, the plateau value of pressure gradient tends to last longer for larger gas slugs.

4.3 Radial-flow Model

The radial-flow model assumes that the core scale behaviour can be scaled up directly to field and various banks propagate from the injection well radially with the same dimensionless velocities and mobilities as in the linear core-flood experiments [7].

The wellbore radius (r_w) is 0.1m. The outer radius (r_e) is 20 m, which corresponds to the equivalent well-block radius of a 100 m x 100 m containing the well. The thickness of the region (h) is 1 m. The porosity ϕ is 0.2 and the permeability 150 [mD], as in the linear-flow model. The total mobilities and dimensionless propagation velocities, are those from the linear-flow model, obtained from experimental data. The dimensionless gas and liquid slug sizes are expressed in terms of the pore volume of a 100 m x 100 m x 1m grid block.

For the gas-injection period, the pressure difference is the sum of the pressure differences in the foam bank and the foam-collapse bank. For the liquid-injection period, the total pressure difference is the sum of the pressure differences in the foam-collapse bank, the gas dissolving bank, the liquid fingering bank and the foam bank. By applying the Darcy's law for radial multi-phase flow, the dimensionless pressure difference is calculated for each bank as follows:

$$\Delta P_b = \int_{r_1}^{r_2} \frac{Q_t}{2\pi r h \lambda_t(b)} dr = \frac{Q_t}{2\pi r h \lambda_t(b)} ln \frac{r_2}{r_1}$$

where, in each bank, extending from r_1 to r_2, the total mobility is assumed to be uniform and constant. For the radial-flow model, the dimensionless pressure difference between r_w and r_e is compared to the dimensionless pressure difference caused by injecting water at the same volumetric rate into a fully water saturated region. Then the dimensionless pressure difference P_D is calculated as:

$$\Delta P_D = \frac{\Delta_P}{(\Delta P_t)_{sw=1}} = \frac{\Delta p_t}{\frac{Q_t}{q\pi r h \lambda w} ln \frac{r_e}{r_w}}$$

where λ_w is the water mobility of a fully water-saturated region (S_w=1)

4.4 Results for Radial-flow Model

4.4.1 Effect of gas velocity

Figure 4.11(a) shows the dimensionless pressure drop as a function of total pore volumes of gas injected at 1 ml/min flow rate. During this period the foam-collapse bank propagates from the injection well. Figure 4.11(b) represents the dimensionless pressure drop from the injection well

using the laboratory data for gas injection at 1 ml/min. The pressure drop decreases as the foam collapses in each region.

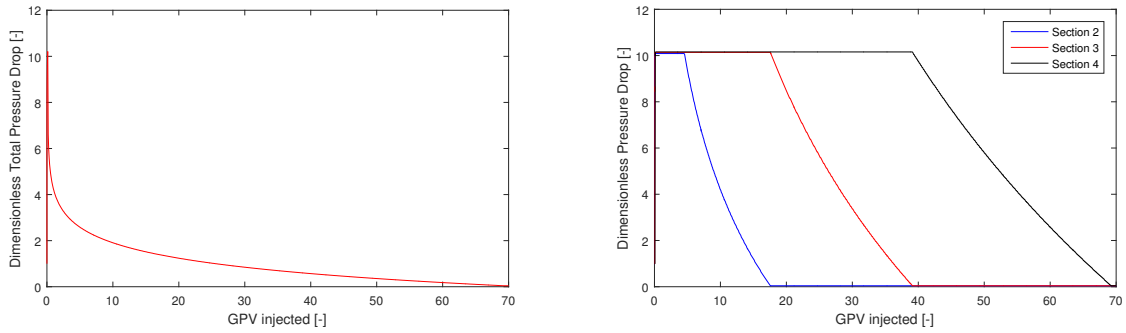

(a) (b)

Figure 4.11: Dimensionless pressure drop surrounding the injection well using the data from the core-flood with gas injection at 1 ml/min(4.11(a)), and dimensionless pressure drop in three regions of increasingly distance from the injection well during gas injection 4.11(b)

Figure 4.12(a) shows the dimensionless pressure as a function of total pore volume injected using the data from the core-flood with gas injection at 2 ml/min. As can be seen, the pressure decreases as more gas is injected; this represents the foam-collapse propagation from the injection well. Compared to the previous gas injection at 1 ml/min, this case takes slightly fewer pore volumes to collapse the foam. Figure 4.12(b) represents the pressure drop in three regions of increasingly distance from the injection well. The foam-collapse bank propagates outward from the injection well.

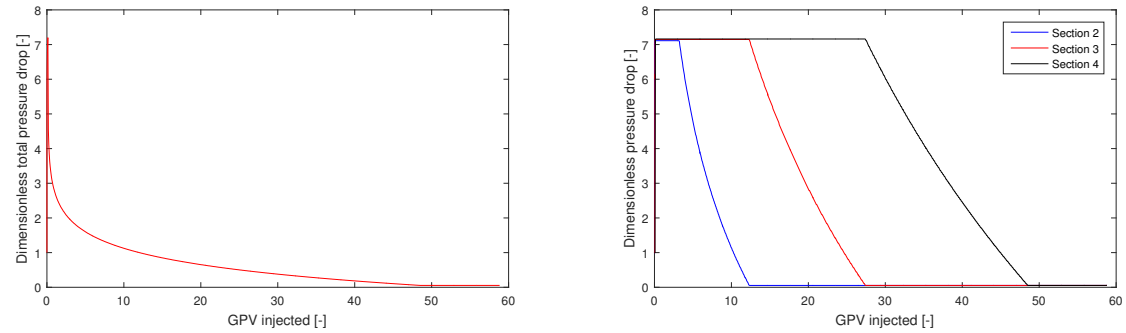

(a) (b)

Figure 4.12: Dimensionless pressure drop surrounding the injection well using the data from the core-flood with gas injection at 2 ml/min(4.12(a)) and dimensionless pressure drop in three regions of increasingly distance from the injection well during gas injection 4.12(b)

As shown in figure 4.13, the collapse-foam bank propagates from the injection as gas is injected using the lab data for gas injection at 3 ml/min. The trend is similar to those using the data for gas injection at 2 ml/min. The peak in the dimensionless pressure drop is 7. The difference in the peaks of dimensionless pressure gradient is small among all the injection rates. The dimensionless pressure drops at similar number of grid-pore volumes injected (GPV).

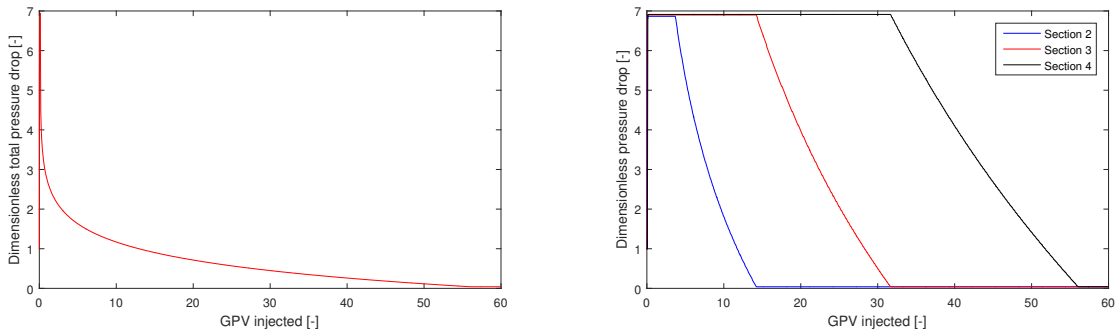

(a) (b)

Figure 4.13: Dimensionless pressure drop surrounding the injection well using the data from the core-flood with gas injection at 3 ml/min (4.13(a)) and dimensionless pressure drop in three regions of increasingly distance from the injection well during gas injection (4.13(b))

4.4.2 Effect of liquid velocity

Figures 4.14, 4.15 and 4.16 show the dimensionless pressure drop surrounding the injection well during the liquid injection period using laboratory data at different flow rates. The predicted dimensionless pressure drop in radial-flow decreases as the liquid flow rate in the lab experiment increases. Once predicted liquid injection starts, the pressure rises to a plateau followed by a decrease in pressure.

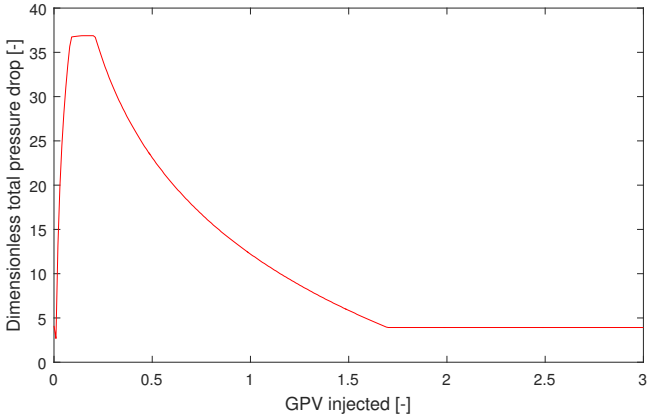

Figure 4.14: Dimensionless Pressure drop surrounding the injection well using laboratory data taken at liquid injection 0.5 ml/min

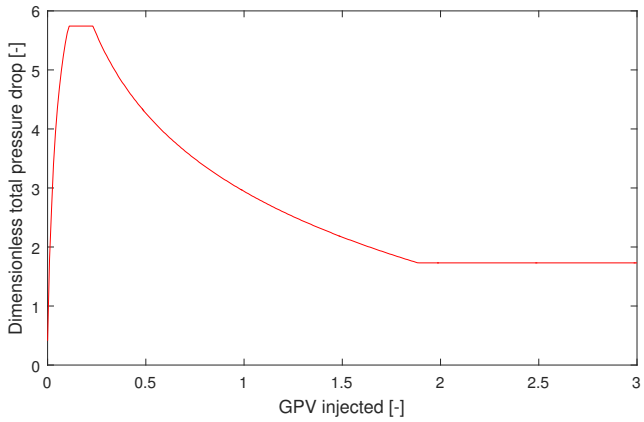

Figure 4.15: Dimensionless pressure drop surrounding the injection well using laboratory data taken at liquid injection 5 ml/min

Figure 4.16 shows the dimensionless pressure drop surrounding the injection well during the liquid injection at 50 ml/min. Following the plateau, pressure starts to decline gradually, the trend is not as steep as with lower flow rates. The reason could be that since the flow rate is too high, the liquid saturates quickly the foam-collapse region and then then following regions so the mobilities and velocities of the gas dissolving bank and the liquid fingering are similar. There is a huge effect of liquid injection rate, approximately 25 times difference in pressure rise at well, from 0.5 ml/min to 50 ml/min.

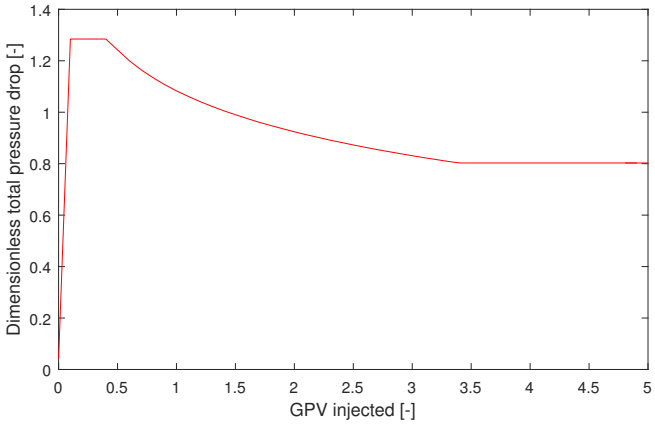

Figure 4.16: Dimensionless pressure drop surrounding the injection well using laboratory data taken at liquid injection 50 ml/min

4.4.3 Effect of gas slug size on subsequent liquid injection

Figure 4.17 compares the dimensionless pressure drop surrounding the injection during the liquid injection following various periods of gas injection. A large amount of gas improves the subsequent liquid injectivity, similar to the trend observed with the linear-flow model. The bigger the gas-slug size, the better the subsequent liquid injectivity.

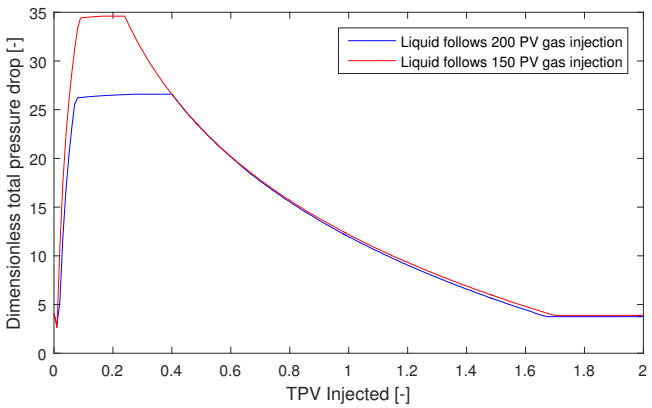

Figure 4.17: Dimensionless pressure drop surrounding the injection well using the lab data taken at the liquid injection period

4.5 Comparison between Radial-Flow Model and Simulation based on Peaceman Equation

The Peaceman equation is used in most finite-difference simulators. It describes the pressure difference between the injection well and the grid-block containing the injection well [18]. Previous studies [18] reported injectivity errors during gas injection in SAG in simulations based on the conventional Peaceman equation. The equation ignores the rapidly changing saturation around the wellbore caused by the injection of alternating surfactant and gas slugs. [18].

Some assumptions were made for the calculations based on the Peaceman equation:

- Oil is not present in the region of interest
- Water, gas and rock are assumed to be incompressible
- The reservoir is of a uniform height h and the vertical injection well penetrates the entire interval
- The effect of gravity is not considered
- Foam immediately reaches local equilibrium
- The water saturation in the grid block is uniform at all times
- Dispersion and viscous fingering are not considered
- The grid block is assumed to be fully water saturated (S_w=1) at the start of gas injection

The water saturation in the grid-block is determined as a function of time, using a material balance equation on the grid block using the injection well.

This is calculated as follows:

$$Q_i^{in} = Q_w^{out} + Q_g^{out}$$

$$L^2 H \Phi \frac{dS_w}{dt} = Q_w^{in} + Q_g^{out}$$

A wellbore of radius r_w (0.1m) is located in a square grid-block size L x L, which is surrounded by four grid blocks. The grid-block size L is 100 m.

The Upwind-weighting is assumed in the flux determination. The uniform water saturation of the central grid block (S_{wb}) is calculated as follows:

$$L^2 H\Phi \frac{dS_w}{dt} = Q_w^{in}(f_w^{in} - f_w(S_{wb}))$$

where f_w^{in}=0 for gas injection and f_w^{in}=1 for liquid injection.

The pressure difference between the injection well and the grid block ΔP_t is calculated as follows:

$$P_{re} = P_b$$

$$\Delta P_t = P_w - P_{re}$$

$$= \frac{Q_i^{in}}{2\pi hk\lambda_{rt}} ln \frac{r_e}{rw}$$

4.5.1 Effect of gas velocity

Figure 4.18 compares the dimensionless pressure drop calculated with the Peaceman equation and the radial-flow model. This figure shows that the gas injectivity is underestimated with the Peaceman equation, especially for the minimum values at the later stage of the injection. The peak of the dimensionless pressure drop calculated with the Peaceman equation is around 1000, which is much higher than the value calculated with the radial-flow model.

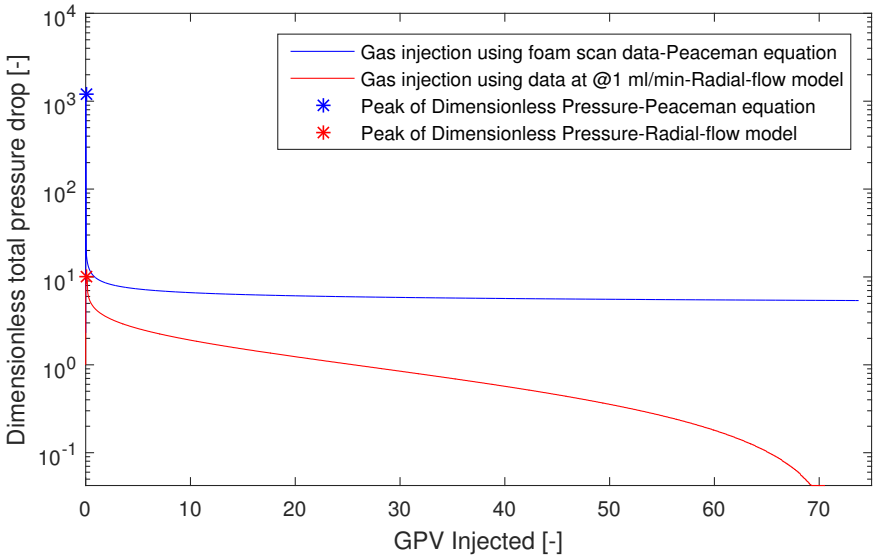

Figure 4.18: Comparison of gas injectivity calculated with the Peaceman equation and the radial-flow model using core-flood data for gas injection at 1 ml/min

Figure 4.19 compares gas injectivity with the radial-flow model using data at 2 ml/min and Peaceman equation. The dimensionless pressure drop is overestimated with the Peaceman equation.

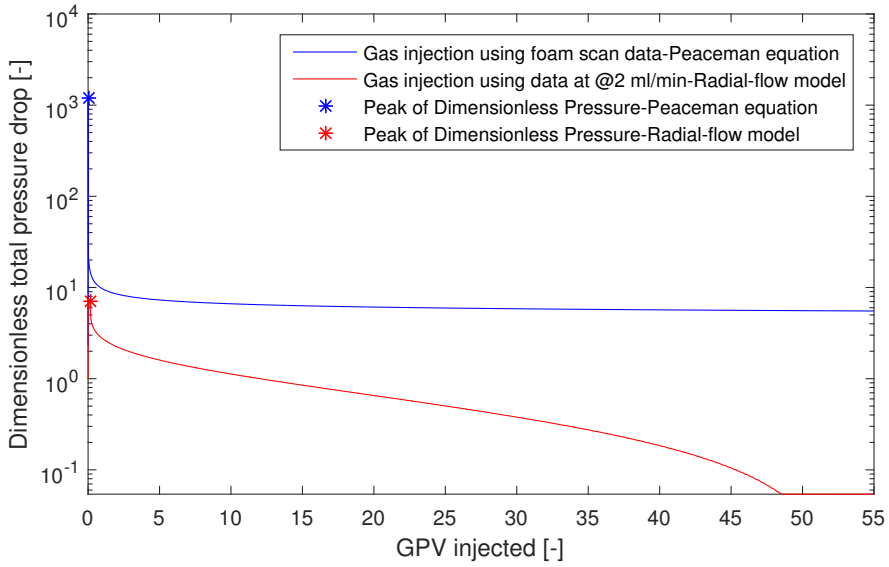

Figure 4.19: Comparison of gas injectivity calculated with the Peaceman equation and the radial-flow model using core-flood data for gas injection at 2 ml/min

As shown in Figure 4.20, gas injectivity is again overestimated with the Peaceman equation compared to the radial flow-model based on data at 3 ml/min.

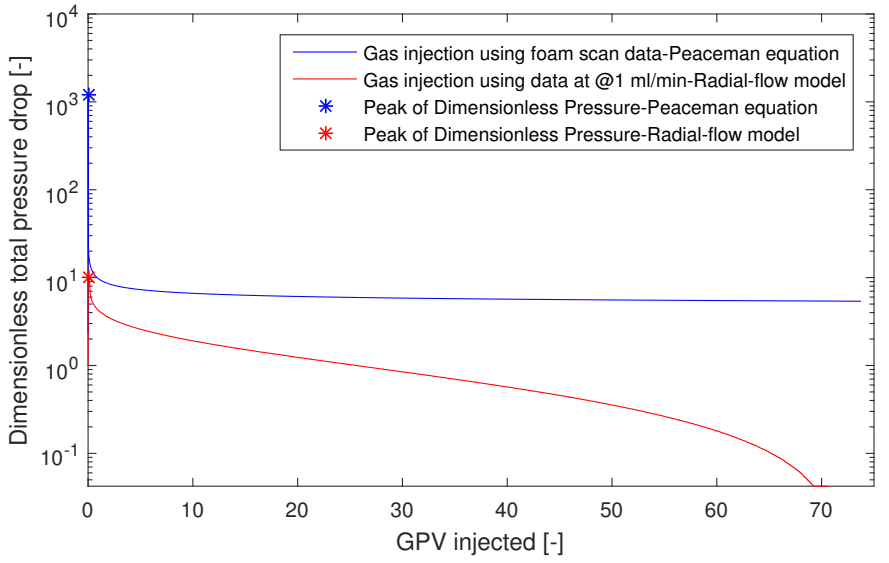

Figure 4.20: Comparison of gas injectivity calculated with the Peaceman equation and the radial-flow model using core-flood data for gas injection at 3 ml/min

Figure 4.21 summarizes the results of the calculation of dimensionless pressure using lab data for gas injection at different flow rates using the radial-flow model and the Peaceman equation. The dimensionless pressure drop calculated using the radial-flow model varies depending on the gas injection flow rate in the experiment. This difference is most visible between data taken at 1 ml/min and 2 ml/min injection rates.

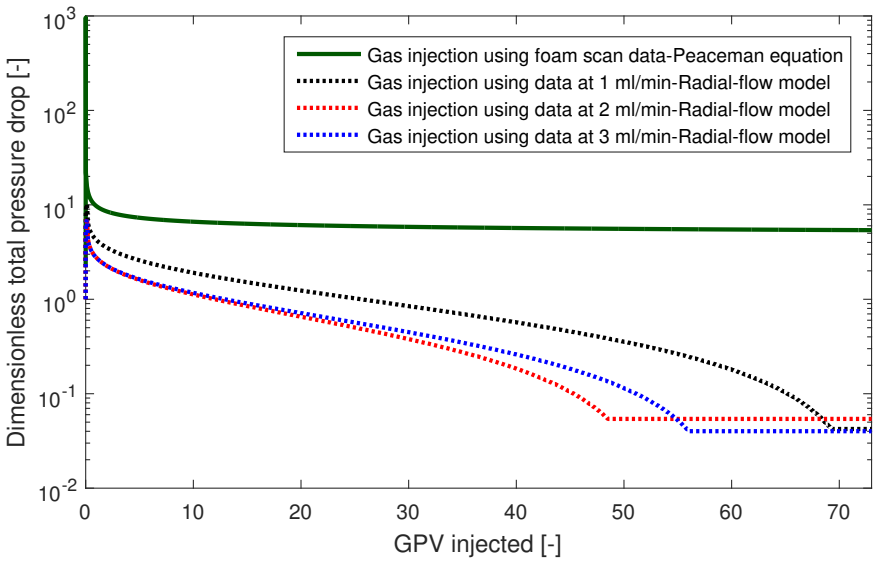

Figure 4.21: Comparison of gas injectivity calculated with the Peaceman equation and the radial-flow model using core-flood data for gas injection at different flow rates

4.5.2 Effect of liquid velocity

Figure 4.22 compares the simulation using the Peaceman equation and the radial-flow model using data for liquid injection at 0.5 ml/min. As shown in this figure, using the Peaceman equation underestimates the liquid injectivity by around 30 times at the peak of the dimensionless pressure drop.

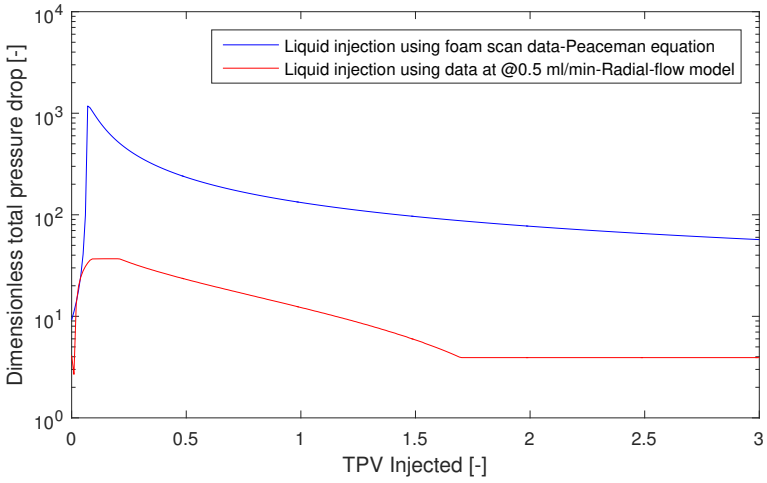

Figure 4.22: Comparison of liquid injectivity calculated with the Peaceman equation and the radial-flow model using core-flood data for liquid injection at 0.5 ml/min

Figure 4.23 compares the dimensionless pressure drop calculated with the radial-flow model with data for 5 ml/min injection rate and the simulation using Peaceman equation. Similar to the previous case, liquid injectivity is underestimated by more than 100 times at the peak of the dimensionless pressure.

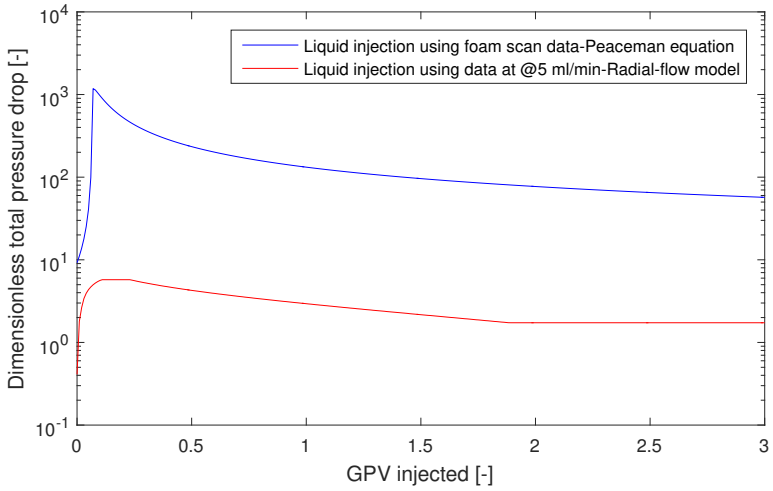

Figure 4.23: Comparison of liquid injectivity calculated with the Peaceman equation and the radial-flow model using core-flood data for liquid injection at 5 ml/min

Figure 4.24 compares the dimensionless pressure calculated with the Peaceman equation and with the radial-flow model with data for liquid injection at 50 ml/min. After the dimensionless pressure drop reaches the peak, the pressure holds nearly constant during subsequent injection.

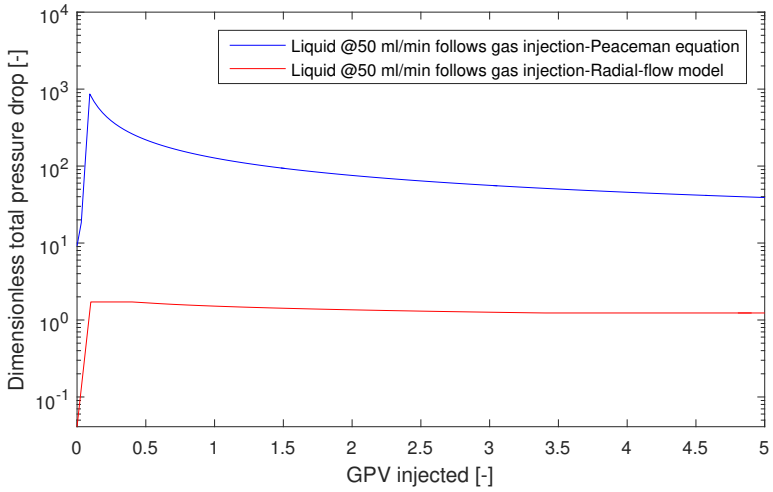

Figure 4.24: Comparison of liquid injectivity calculated with the Peaceman equation and the radial-flow model using core-flood data for liquid injection at 50 ml/min

As shown in figure 4.25 the liquid injectivity is underestimated by the Peaceman equation. As the flow rate increases the error becomes larger.

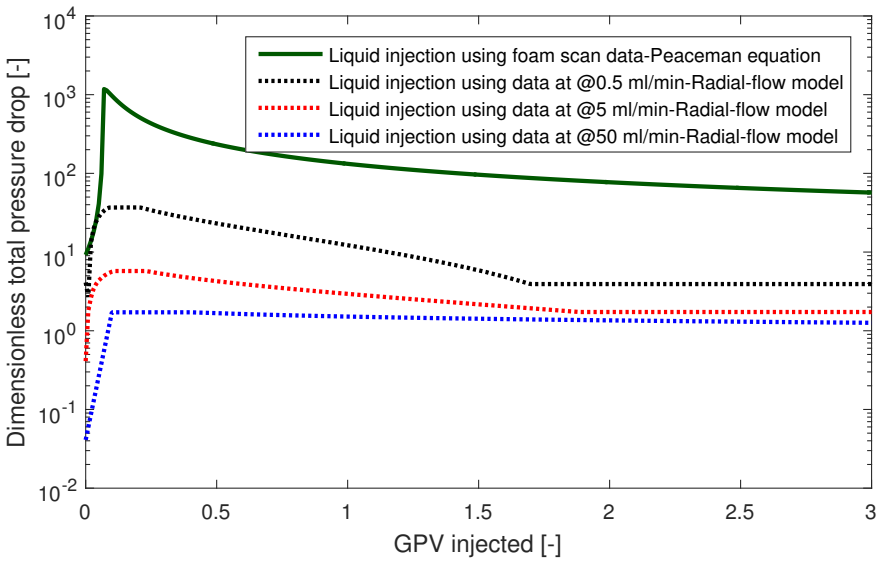

Figure 4.25: Comparison of the pressure gradient calculated with Peaceman-equation and the radial-flow model using the core-flood data for liquid injection following at different injection rates.

4.5.3 Effect of gas slug size on subsequent liquid injectivity

Similar to the results shown during the liquid and gas injection, the liquid dimensionless pressure drop during liquid injection following different periods of gas injection is overestimated with the Peaceman equation. The only difference between Figure 4.26 and 4.27 is the size of the slug previously injected. The model accounts for this, the mobilities are quite similar but the length of the foam-collapse region is slightly larger after 200 GPV injected compared to the region after 150 GPV.

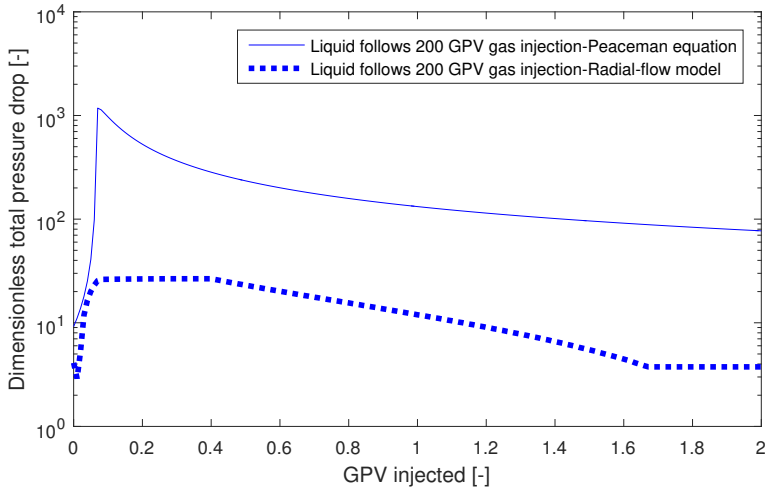

Figure 4.26: Comparison of liquid injectivity calculated with the Peaceman equation and the radial-flow model using the core-flood data for liquid injection following 200 PV gas injected.

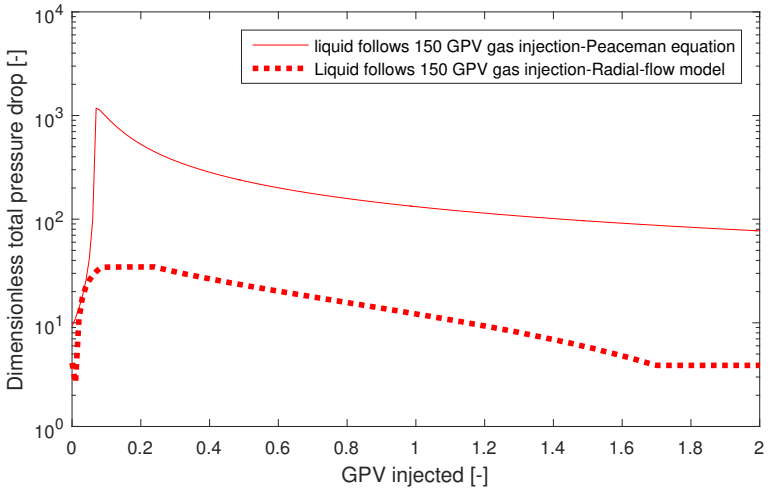

Figure 4.27: Comparison of liquid injectivity calculated with the Peaceman equation and the radial-flow model using the core-flood data for liquid injection following 150 PV gas injected

Figure 4.28 represents the comparison of the liquid injectivity. In the radial-flow model, the size of the gas slug has an effect on the subsequent liquid injection. The larger the size of the slug the better the injectivity during the subsequent liquid injection. This was confirmed during the core-flood experiments where different gas slug sizes were injected before the liquid injection. The effect of the previous slug gas on the subsequent following liquid injection is not represented by the models based on the Peaceman equation. The dimensionless pressure drop calculated by the Peaceman equation is the same in both cases since the foam parameters used in the simulation are taken at one initial state.

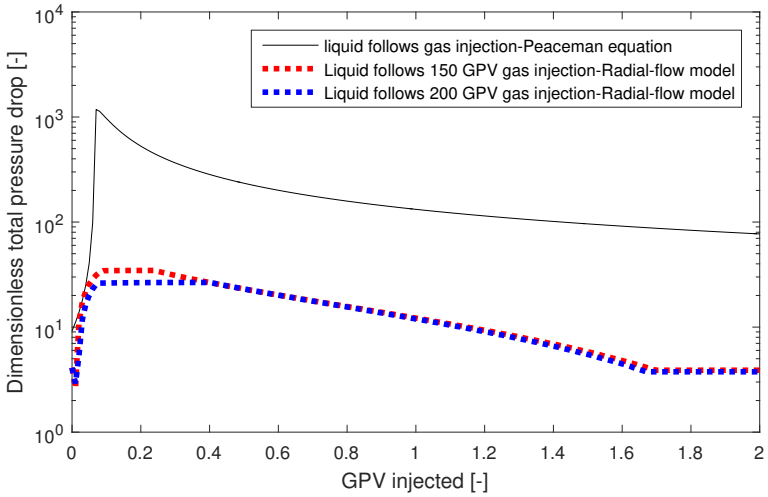

Figure 4.28: Comparison of liquid injectivity calculated with the Peaceman equation and the radial-flow model using the core-flood data for liquid injection following different volumes of gas injected

The linear model gives a good fit to the experimental data taken for gas injection at different injection velocities. Based on this fit, the dimensionless velocity and the mobility at each flow rate were calculated to extrapolate from the core scale to the flow around the injection well. Results show that the conventional simulator using the Peaceman equation underestimates gas and liquid injectivity. Two of the reasons for underestimation of liquid injectivity are liquid fingering through foam and gas dissolving into liquid; these effect are not included in the foam simulator model.

In simulation of gas injection with Peaceman equation, combined with the assumption of uniform

saturation in the injection-well grid block, leads to underestimation of injectivity. The magnitude of this effect decreases as the simulation grid is refined around the well, resulting in longer simulation times. Therefore, grid resolution around injection well is important in modelling SAG Foam EOR processes.

Moreover, conventional models cannot represent the effect of the gas previously injected on the subsequent liquid injectivity, especially the propagation of the foam-collapse region. Fingering of liquid through gas is important to the liquid injectivity but hard to represent in the simulator. The model is based on experimental results, which depends on temperature, pressure surfactant formulation, porous media, etc. A new set of experiments would needed to be conducted to calculate parameters and fit the data to the model for each field application.

Chapter 5

Conclusions and recommendations

5.0.1 Conclusions

For the cases investigated in this study, conclusions are made as follows:

- Gas-injection velocity has no big impact on foam collapse. Somewhat shear thinning behaviour has been observed in gas mobility during gas injection.
- The foam collapse reflects the combined effects of pressure driven flow, capillary effect and an important effect of liquid evaporation.
- During liquid injection, the trend suggest a shear-thinning behaviour.
- The increment in injection velocity is not proportional to the increment in pressure gradient.
- 'Regardless of injection velocity, the dissolution of gas in liquid starts roughly at the same number of pore volumes liquid injected.
- A prolonged period of gas injection forms a region near to the inlet crucial to injectivity.
- The bigger the gas slug size the better the subsequent liquid injectivity.
- Beyond the foam-collapse region, the effect of the gas slug size is not visible. The plateau of pressure gradient is similar in all cases but is lasts longer as more gas was previously injected suggesting a longer period of time needed to dissolve the gas.
- It is expected that liquid finger are wider if liquid is injected at a higher velocity.
- Foam quality has no significant effect on the subsequent liquid and gas injection.
- Pressure gradient tend to be higher during gas gas injection following foam 0.60 foam-quality.
- Conventional models based on the Peaceman equation underestimates liquid and gas injectivity. They cannot represent the effect of previous gas injection on the subsequent liquid injection. Hysteresis is absent from models.

5.0.2 Recommendations

The recommendations are made as follows:

- Further experiments can be conducted to investigate the effect of permeability.

- Effect of liquid velocity during liquid injection can be verified through CT scan experiments.
- Injectivity model can be improved to account for the effect of different propagation velocities in each section.
- The real injectivity is better than the predicted by the simulator. However, the radial-flow model is based on laboratory experiments, which include many assumptions ans simplifications. A new set of experiments would need to be conducted to calculate parameters and fit the data to the model for each field application.

Chapter 6

Appendix

6.1 Permeability Test

At the beginning of the experiments the permeability of the core was measured. Several flow rates were injected in the core and the pressure response was recorded. First increasing values and subsequently decreasing values. The flow rates tested were 0.5, 1, 2, 3, 4 and 5 ml/min. By using Darcy's equation, the permeability was calculated. This by plotting the recorded data of Q/A versus $\nabla P/\mu L$.

where A is the cross-sectional area of the core [m^2] and μ is the viscosity of the brine at 90°C[Pa·s].

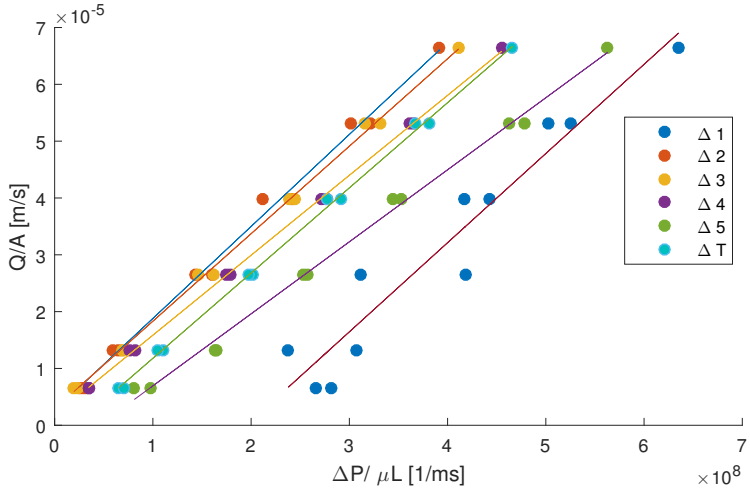

Figure 6.1: Permeability test for Berea core

Permeability is then obtained from the slope of the linear trend of each section.

Line equation of each section :

$$m_1 = 1.569e-13$$

$$m_2 = 1.619e-13$$

$$m_3 = 1.569e-13$$

$$m_4 = 1.407e-13$$

$$m_5 = 1.268e-13$$

$$m_T = 1.500e-13$$

Then the permeability in the core is 1.50e-13 [m^2] or 150 [mD]

6.2 Relative Permeability of water and gas

In this study the relative permeability functions of water and gas are defined as:

$$k_{rw}(S_w) = k^0_{rw}\left(\frac{S_w - S_{wc}}{1 - S_{wc} - S_{gr}}\right)^{nw}$$

$$k_{rg}(S_w) = k^0_{rg}\left(\frac{1 - S_w - S_{gr}}{1 - S_{wc} - S_{gr}}\right)^{ng}$$

where k_{rw} and k_{rg} are water and gas relative permeabilities, respectively. n_w and n_g are the empirical parameters, k^0_{rw} and k^0_{rg} are the end-point water and gas relative permeabilities, respectively. Their values are listed in table 6.1, these parameter values were reported by Kapetas et al [11]. Water and gas viscosities are 3.2e-4 [Pa·s] and 2e-5 [Pa·s], respectively.

Table 6.1: Corey Parameter

Parameter	Units	Value
n_g	-	1.22
n_w	-	5.25
k^0_{rg}	-	0.47
k^0_{rw}	-	0.14
S_{gr}	-	0.24
S_{wr}	-	0.204

6.3 Foam Scan

The following figures show the foam scan in section 2 and 3 at 2 ft/day.

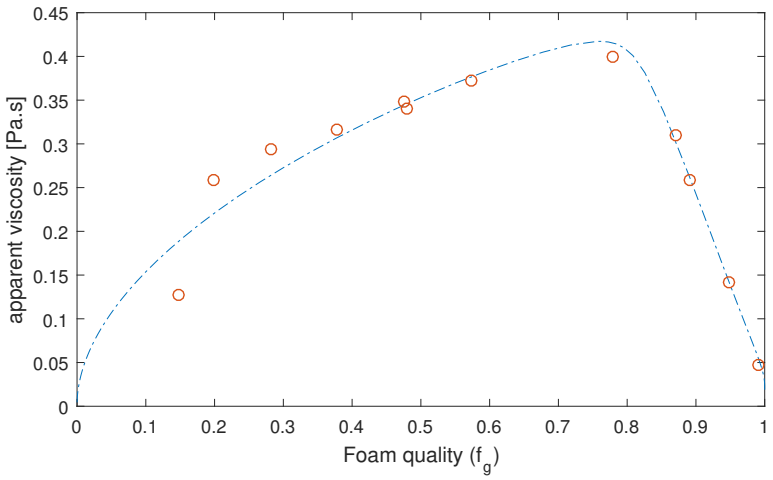

Figure 6.2: Apparent viscosity as a function of gas fraction at 2 ft/day in section 2.

Table 6.2: Foam model-parameters obtained by fitting the least-square fitting approach to the foam scan at 2 ft/day in section 2

Parameter	Units	Value
fmdry	-	0.352
epdry	-	394.5
fmmob	-	1.375e5
epcap	-	0.999
fmcap	-	6.626e-6

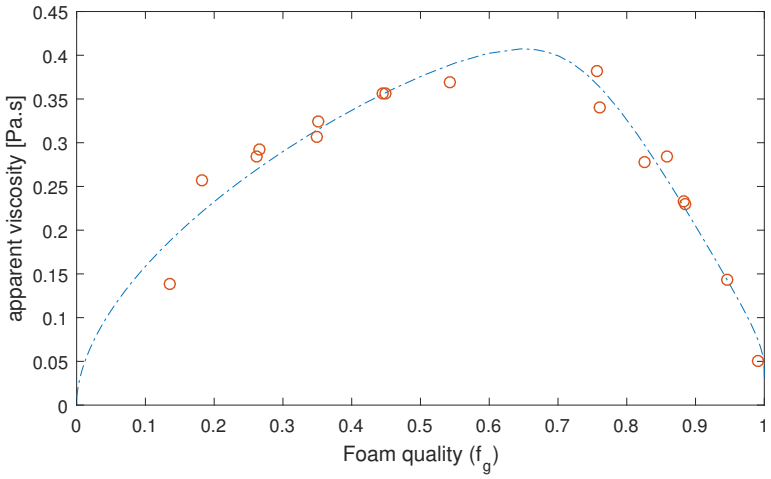

Figure 6.3: Apparent viscosity as a function of gas fraction at 2 ft/day in section 3.

Table 6.3: Foam model-parameters obtained by fitting the least-square fitting approach to the foam scan at 2 ft/day in section 3

Parameter	Units	Value
fmdry	-	0.365
epdry	-	454.0.30
fmmob	-	1.375e5
epcap	-	0.879
fmcap	-	6.347e-6

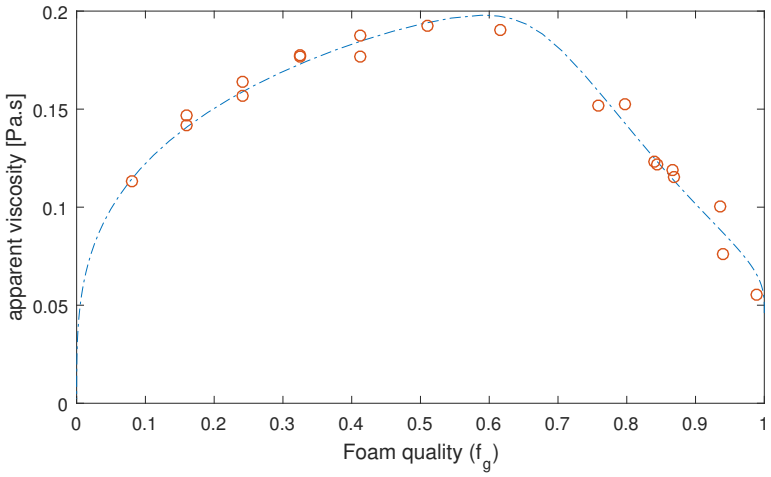

Figure 6.4: Apparent viscosity as a function of gas fraction at 4 ft/day in section 2.

Table 6.4: Foam model-parameters obtained by fitting the least-square fitting approach to the foam scan at 4 ft/day in section 2

Parameter	Units	Value
fmdry	-	0.365
epdry	-	454.0.30
fmmob	-	1.375e5
epcap	-	0.879
fmcap	-	6.347e-6

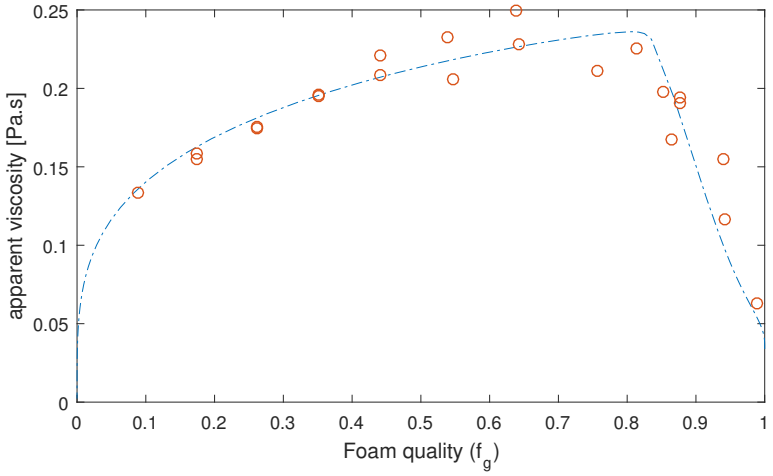

Figure 6.5: Apparent viscosity as a function of gas fraction at 4 ft/day in section 3.

Table 6.5: Foam model-parameters obtained by fitting the least-square fitting approach to the foam scan at 4 ft/day in section 3

Parameter	Units	Value
fmdry	-	0.413
epdry	-	343.5
fmmob	-	2.79e4
epcap	-	0.42
fmcap	-	9.037e-6

Nomenclature

ΔP	pressure drop across core cross-sectional, Pa
μ_{app}	apparent viscosity, Pa·s
μ_g	gas viscosity, Pa·s
∇p	pressure gradient, Pa/m
ϕ	porosity, [-]
ρ_g	density of gas, [kg/m^2
σ_{wg}	gas/water surface tension
f_g	gas fractional flow
k	permeability, m^2
k^0_{rg}	end-point gas relative permeability, [-]
k^0_{rw}	end-point water relative permeability [-]
k_{rg}	relative permeability to gas without foam
k_{rg}	relative permeability to gas
k^f_{rg}	relative permeability to gas with foam
k_{rw}	relative permeability to water
n_g	Corey exponent of gas, [-]
n_w	Corey exponent of water [-]
P_c*	Limiting capillary pressure
S_or	Residual Oil saturation
S_w*	Water saturation at which foam collapses
S_{gr}	residual gas saturation, [-]
S_{wr}	resiadual water saturation. [-]
u_t	total superficial velocity, m/s
A	area, m^2
epcap	captures the shear thinning behaviour of the low quality regime
epdry	parameter controlling the abruptness of the foam collapse

fmmob reference gas mobility reduction for wet foams

k permeability, m^2

L length of the core, m

LPV Local Pore Volume

Q flow rate, m^3/s

TPV Total Pore Volume

Bibliography

[1] J.M. Alvarez, H.J. Rivas, and W.R.Rossen. Unified model for steady-state foam behaviour at high and low foam qualities. *SPE*, pages 1–12, 1999. doi: https://doi.org/10.2118/56825-MS.

[2] A.R.Kovscek and C.J. Radke. *Fundamentals of Foam Transport in Porous Media*. ACS Advances in Chemistry series 242, Washington DC, 1994.

[3] C.S. Boeije and W.R. Rossen. Gas Injection Rate Needed for SAG Foam Processes to Overcome Gravity Override. *SPE*, pages 1–10, 2013. doi: https://doi.org/10.2118/166244-MS.

[4] L. Cheng, A.B. Reme, D. Shan, D.A. Coombe, and W.R. Rossen. Simulating Foam Processes at High and Low Quality Regime. *SPE*, pages 1–15, 2000. doi: https://doi.org/10.2118/59287-MS.

[5] A. Faisal, K. Bisdom, B. Zhumabek, and W.R. Rossen. Injectivity and Gravity Segregation in WAG and SWAG Enhanced Oil Recovery. *SPE*, pages 1–7, 2009. doi: https://doi.org/10.2118/124197-MS.

[6] R. Farajzadeh, A.A Eftekhari, H. Hajibeygi, J.M. van der Meer, S.Vincent-Bonnieu, and W.R.Rossen. Simulation of instabilities and Fingering in Surfactant Alternating Gas (SAG) Foam Enhanced Oil Recovery. *SPE*, pages 1–18, 2015. doi: https://doi.org/10.2118/173193-MS.

[7] J. Gong, S.Vincent-Bonnieu, R.Z. Kamarul, J. Groenenboom, R. Farajzadeh, and W.R.Rossen. Modelling of Liquid Injectivity in Surfactant-Alternating-Gas Foam Enhanced Oil Recovery. *SPE*, pages 1–19, 2018. doi: https://doi.org/10.2118/190435-MS.

[8] Don W. Green and Willhite G. Paul. Enhanced Oil Recovery. *SPE*, 6:561, 1998.

[9] Computer Modelling Group. Stars user's guide, version 201.2.2010, 2010.

[10] G.J. Hirasaki, C.A. Miller, R. Szafranski, D. Tanzil, and J.B. Lawson. Field Demonstration of the Surfactant/Foam Process for Aquifer Remediation. *SPE*, pages 1–16, 1997. doi: https://doi.org/10.2118/39292-MS.

[11] L. Kapetas, S.Vincent-Bonnieu, R. Farajzadeh, A.A. Eftekhari, S.R. M, and W.R.Rossen. Effect of permeability on Foam-model parameters-An Integral Approach from Core-flood Experiments through to Foam Diversion Calculation. *Colloids and Surfaces A: Physicochemical and Engineering Aspects*, pages 172–180, 2017.

[12] Z.I. Kathib, G.J. Hirasaki, and A.H.Falls. Effects of Capillary Pressure on Coalescence and Phase Mobilities in Foams Flowing Through Porous Media. *SPE*, 3(03):1–8, 1988. doi: https://doi.org/10.2118/15442-PA.

[13] K.E.Thompson and R.D. Gdanski. Laboratory Study Provides Guidelines for Diverting Acid with Foams. *SPE*, pages 1–6, 1993. doi: https://doi.org/10.2118/23436-PA.

[14] K.R Kibodeaux, W.R. Rossen, J.-X. Shi, and M.T Lim. Injectivity and Gravity Override in Surfactant-Alternating-Gas Foam Processes. *SPE*, pages 1–12, 1995. doi: https://doi.org/10.2118/30753-MS.

[15] Donald L. Kuehne, Deborah I Ehman, Alan S. Emanuel, and Charles F. Maganani. Design and Evaluation of a Nitrogen-Foam Field Trial. *SPE*, pages 1–9, 1990. doi: https://doi.org/10.2118/17381-PA.

[16] Larry W. Lake. *Enhanced Oil Recovery*. Prentice Hall, Upper Saddle River, New Jersey, 1989.

[17] Larry W. Lake, Russell Johns, Bill Rossen, and Gary Pope. *Fundamentals of Enhanced Oil Recovery*. SPE, 2014.

[18] T.N. Leeftnik, C.A. Latooij, and W.R.Rossen. Injectivity errors in simulation of foam EOR. *Journal of Petroleum Science and Engineering*, pages 1–9, 2015.

[19] Robert Feng Li, Wei Yan, Shunhua Liu, George J. Hirasaki, and Clarence A. Miller. Foam Mobility Control for Surfactant Enhanced oil Recovery. *SPE*, pages 1–15, 2010. doi: https://doi.org/10.2118/113910-PA.

[20] K. Ma, J.Lopez-Salinas, M. Puerto, and G.J. Hirsaki. Estimation of Parameter for the Simulation of Flow through Porous Media. Part 1: The dry Out Effect. *Energy and Fuels*, pages 2363–2375, 2013.

[21] MP3. Tu delft (version 3), 2016.

[22] Quoc P. Nguyen, Peter K. Curie, and Pacelli L.J. Zitha. Determination of Foam Induced Fluid Partitioning in Porous Media using X-Ray Computed Tomography. *SPE*, pages 1–7, 1982. doi: https://doi.org/10.2118/80245-MS.

[23] Quoc P. Nguyen, P.K.Currie, W.R. Rossen, and Pacelli L.J. Zitha. CT Study of Liquid Diversion With Foam. *SPE*, pages 1–21, 2005. doi: https://doi.org/10.2118/94764-PA.

[24] Quoc P. Nguyen, W.R. Rossen, and Pacelli L.J. Zitha. Determination of Gas Trapping with Foam Using X-Ray Computed Tomography and Effluent Analysis. *SPE*, pages 1–15, 2009. doi: https://doi.org/10.2118/94764-PA.

[25] W.T. Osterloh and M.J Jante Jr. Effects of Gas and Liquid Velocity on Steady-State Foam Flow at High Superficial Velocity. *SPE*, pages 1–12, 1992. doi: https://doi.org/10.2118/24179-MS.

[26] T.W. Patzek. Field applications of Foam for Mobility Improvement and Profile Control. *SPE*, pages 1–7, 1996. doi: https://doi.org/10.2118/29612-PA.

[27] Q.Xu and W.R.Rossen. Experimental Study of Gas Injection in a Surfactant-Alternating-Gas Foam Process. *SPE*, pages 1–11, 2004. doi: https://doi.org/10.2118/84183-PA.

[28] C.J. Radke and J.V. Gillis. A Dual Tracer Technique for Determining Trapped Gas Saturation during Steady Foam Flow in Porous Media. *SPE*, pages 1–8, 1990. doi: https://doi.org/10.2118/20519-MS.

[29] R.A.Kil, Q.P. Nguyen, and W.R. Rossen. Determining Trapped Gas in Foam From CT Images. *SPE*, pages 1–13, 2009. doi: https://doi.org/10.2118/124157-MS.

[30] W.J. Renkema and W.R. Rossen. The Apparent Viscosity of Foams in Homogeneous Bed Packs. *SPE*, pages 1–10, 1989. doi: https://doi.org/10.2118/16048-PA.

[31] W.J. Renkema and W.R. Rossen. Success of SAG Foam Processes in Heterogeneous Reservoir. *SPE*, pages 1–28, 2007. doi: https://doi.org/10.2516/ogst:2007060.

[32] Tomas Sara. Enhanced Oil Recovery-An Overview. *Oil & Gas Science and Technology*, 63:9–19, 2008. doi: https://doi.org/10.2516/ogst:2007060.

[33] D. Shan and W.R. Rossen. Improved Surfactant-Alternating-Gas Foam Process for SAG Foam Processes to Control Gravity Override. *SPE*, pages 1–19, 2004. doi: https://doi.org/10.2118/88811-PA.

[34] J.-X. Shi and W.R. Rossen. Improved Surfactant-Alternating-Gas Foam Process for SAG Foam Processes to Control Gravity Override. *SPE*, pages 1–8, 1998. doi: https://doi.org/10.2118/39653-MS.

[35] L.L Shramm. Foams: Fundamentals and applications in the petroleum industry. *American Chemical Society*, 3(242), 1994.

[36] D.H. Smith and S.A. Jikich. Foams and Surfactants for Improved Underground Storage of Natural Gas by Blockage of Water Coning. *SPE*, pages 1–5, 1993. doi: https://doi.org/10.2118/26908-MS.

[37] W.R. *Foam in Enhanced Oil Recovery*. New York:Marcel Dekker, 1996.

[38] S.C Zeilinger, M.Wang, and R. Kibodeaux. Improved Prediction Of Foam Diversion in Matrix Acidization. *SPE*, pages 1–13, 1995. doi: https://doi.org/10.2118/29529-MS.